NAVAL POSTGRADUATE SCHOOL
Monterey, California

THESIS

CHARACTERIZATION OF MICROSTRUCTURE AND MICROTEXTURE IN LONGITUDINAL SECTIONS FROM FRICTION STIR PROCESSED NICKEL-ALUMINUM BRONZE

by

Kenneth Brent Faires

June 2003

Thesis Advisor: Terry R McNelley

Approved for public release; distribution is unlimited

THIS PAGE INTENTIONALLY LEFT BLANK

REPORT DOCUMENTATION PAGE

Form Approved OMB No. 0704-0188

1. AGENCY USE ONLY *(Leave blank)*	2. REPORT DATE	3. REPORT TYPE AND DATES COVERED
	June 2003	Master's Thesis

4. TITLE AND SUBTITLE **Characterization of Microstructure and Microtexture in Longitudinal Sections from Fiction Stir Processed Nickel-Aluminum Bronze**

5. FUNDING NUMBERS

6. AUTHOR (S) Faires, Kenneth B

7. PERFORMING ORGANIZATION NAME(S) AND ADDRESS(ES)
Naval Postgraduate School
Monterey, CA 93943-5000

8. PERFORMING ORGANIZATION REPORT NUMBER

9. SPONSORING / MONITORING AGENCY NAME(S) AND ADDRESS(ES)
N/A

10. SPONSORING/MONITORING AGENCY REPORT NUMBER

11. SUPPLEMENTARY NOTES The views expressed in this thesis are those of the author and do not reflect the official policy or position of the U.S. Department of Defense or the U.S. Government.

12a. DISTRIBUTION / AVAILABILITY STATEMENT
distribution statement

12b. DISTRIBUTION CODE

13. ABSTRACT Cast nickel-aluminum bronze (NAB) is the material of choice for propellers in both surface ships and submarines. New designs require a material with improved strength and hardness while retaining NAB's corrosion resistance. Friction stir processing (FSP) represents a new technology for surface hardening of as-cast NAB by means of severe plastic deformation induced by a rotating tool that is traversed across the surface of a material. FSP can convert a microstructure from a cast to a wrought condition without altering the overall shape of the object being worked. The purpose of this study is to apply recently developed orientation imaging microscopy (OIM) methods to evaluate the influence of FSP on microstructure and microtexture of an as-cast NAB material. Processed material was examined in planes having both longitudinal and transverse orientations with respect to tool motion. Shear textures in the thermomechanically-affected zone (TMAZ) were of particular concern. Results of the analysis of this work will be described and the implications to FSP of NAB propeller materials will be delineated.

14. SUBJECT TERMS	15. NUMBER OF PAGES
Nickel Aluminum Bronze, Friction Stir Processing, Orientation Imaging Microscopy, Energy Dispersive Spectroscopy, Optical Microscopy, Thermomechanically-Affected Zone, Shear Deformation.	77
	16. PRICE CODE

17. SECURITY CLASSIFICATION OF REPORT	18. SECURITY CLASSIFICATION OF THIS PAGE	19. SECURITY CLASSIFICATION OF ABSTRACT	20. LIMITATION OF ABSTRACT
Unclassified	Unclassified	Unclassified	UL

NSN 7540-01-280-5500 **Standard Form 298 (Rev. 2-89) Prescribed by ANSI Std. 239-18**

THIS PAGE INTENTIONALLY LEFT BLANK

Approved for public release; distribution is unlimited

CHARACTERIZATION OF MICROSTRUCTURE AND MICROTEXTURE IN LONGITUDINAL SECTIONS FROM FRICTION STIR PROCESSED NICKEL-ALUMINUM BRONZE

Kenneth Brent Faires
Ensign, United States Navy
B.S., North Carolina State University, 2002

Submitted in partial fulfillment of the
requirements for the degree of

MASTER OF SCIENCE IN MECHANICAL ENGINEERING

from the

NAVAL POSTGRADUATE SCHOOL
June 2003

Author: Kenneth Brent Faires

Approved by: Terry R. McNelley
Thesis Advisor

Young W. Kwon
Chairman, Department of Mechanical Engineering

THIS PAGE INTENTIONALLY LEFT BLANK

ABSTRACT

Cast nickel-aluminum bronze (NAB) is the material of choice for propellers in both surface ships and submarines. New designs require a material with improved strength and hardness while retaining NAB's corrosion resistance. Friction stir processing (FSP) represents a new technology for surface hardening of as-cast NAB by means of severe plastic deformation induced by a rotating tool that is traversed across the surface of a material. FSP can convert a microstructure from a cast to a wrought condition without altering the overall shape of the object being worked. The purpose of this study is to apply recently developed orientation imaging microscopy (OIM) methods to evaluate the influence of FSP on microstructure and microtexture of an as-cast NAB material. Processed material was examined in planes having both longitudinal and transverse orientations with respect to tool motion. Shear textures in the thermomechanically-affected zone (TMAZ) were of particular concern. Results of the analysis of this work will be described and the implications to FSP of NAB propeller materials will be delineated.

THIS PAGE INTENTIONALLY LEFT BLANK

TABLE OF CONTENTS

THIS PAGE INTENTIONALLY LEFT BLANK

LIST OF FIGURES

LIST OF TABLES

THIS PAGE INTENTIONALLY LEFT BLANK

LIST OF ABBREVIATIONS, ACRONYMS, AND SYMBOLS

ASTM	American Society for Testing and Materials
BCC	Body Centered Cubic
CBN	Cubic Boron Nitride
DRX	Dynamically Recrystallized
EBSP	Electron Backscatter Pattern
EDS	Energy Dispersive Spectroscopy
FCC	Face Centered Cubic
FSP	Friction Stir Processing/Processed
HAZ	Heat-Affected Zone
KV	kilovolt
NAB	Nickel Aluminum Bronze
NSWCCD	Naval Surface Warfare Center, Caderock Division
OIM	Orientation Imaging Microscopy
OM	Optical Microscopy
PSN	Particle Stimulated Nucleation
RSC	Rockwell Science Center
SC	Simple Cubic
SEM	Scanning Electron Microscope
TMAZ	Thermomechanically-Affected Zone
TWI	The Welding Institute
UNS	Unified Numbering System
Wt. %	Weight Percent

THIS PAGE INTENTIONALLY LEFT BLANK

ACKNOWLEDGEMENTS

The author would like to express his appreciation to the Defense Advanced Research Projects Agency (DARPA) for their funding and support of this ground-breaking research; Bill Palko and Steve Fielder at the Naval Surface Warfare Center (Caderock Division) for their material and technical support; and last but certainly not least, Murray W. Mahoney at the Rockwell Science Center for his support and contagious enthusiasm.

The author would additionally like to thank Professor Terry McNelley for his input and guidance throughout the course of this research project.

The author would also like to thank Dr. Keichero Oishi for his assistance in the data collection for this project.

Finally the author would like to thank his parents for their unending and unerring support in all of his endeavors.

THIS PAGE INTENTIONALLY LEFT BLANK

I. INTRODUCTION

A. NICKEL-ALUMINUM BRONZE

Nickel-aluminum bronzes (NAB) are copper-based alloys that are commonly used in the casting of components for marine applications. NAB alloys are well suited for such applications because they combine moderate strength with excellent corrosion resistance. Some of their other desirable attributes are [Ref. 1]: i) good fracture toughness at both extremely low and elevated temperatures, combined with moderate tensile strengths; ii) low coefficients of friction and good resistance to wear; iii) non-sparking behavior; iv) high damping capacity; v) and fatigue resistance. These properties are the primary reason for the use of NAB alloys in applications ranging from valves to propellers. The particular interest in this research is the U.S. Navy's use of NAB's for surface ship and submarine propellers.

The alloy typically used for propellers is designated as UNS C95800. This is also known as alpha nickel aluminum bronze or propeller bronze [Ref. 2]. Nickel-aluminum bronze propellers are usually made via sand-casting [Ref. 3] and are then slow-cooled, according to ASTM B148 standard specification for aluminum-bronze sand castings [Ref. 4]. The properties of the material are governed by the complex microstructures that arise when NAB is allowed to cool in such a manner [Refs. 5-6]. Significant variations may arise due to the different cooling rates within the casting. Gas evolution results in porosity and a weakened, less corrosion resistant structure.

Dealloying has been observed in corrosion tests on NAB materials after prolonged immersion in seawater [Refs. 6]. The corrosion resistance may be adversely affected in propeller samples that have been welded. This has also been noted when casting defects that have been repaired via welding. Post-welding annealing treatments have been implemented in order to alleviate the problems caused by welding.

NAB propellers cool very slowly because they comprise thick sections. This results in relatively coarse microstructures and lower yield strengths when compared to the more refined microstructures of wrought materials. Current production processes favor the use of the casting process in manufacture of propellers even though a higher strength and more wear resistant material would obviously be desirable. Such properties are most needed at the propeller surface where cavitation and corrosion damage are initiated. With a satisfactory low-cost process for surface hardening of cast NAB components more efficient and quieter propellers could be manufactured.

B. FRICTION STIR PROCESSING

Friction stir processing (FSP) represents a new technology for microstructure modification and surface hardening of both wrought and cast metals. This study is concerned with application of FSP to cast NAB material. During FSP, a rotating tool interacts with the surface of a given material and, by a combination of sticking and sliding friction, causes local adiabatic heating and

softening of the material and a resultant stirring action. Traversing the rotating tool across the surface of the material allows processing over a defined area. Large plastic deformations in the softened regions are induced by tool rotation, resulting in microstructure refinement and homogenization. Despite the severity of the plastic deformations the overall shape of the original object is maintained. A typically FSP tool consists of an outer cylindrical section containing a pin at the end that is in contact with the material being processed. The pin is centered in the outer section and is the only portion of the tool that actually penetrates the surface of the object being processed. The depth to which microstructure is modified, and thus the depth of hardening, is governed mainly by the length of the pin. The face of the outer cylinder surrounding the pin is referred to as the tool shoulder.

FSP is a solid-state process in which no material is melted. The adiabatic heating is the main source of heating created during tool rotation and is responsible for softening of the affected material during processing. The plastic deformation is so intense that material is transferred from one side of the tool to the other. It is by such large-strain deformation that the tool pin and shoulder effectively forge the material; thus, a region containing a very fine grain structure is created with a single pass of the tool. This region is referred to as the stir zone, or nugget because of its appearance on a transverse section. Just outside the stir zone is a region

that experiences less severe deformation and heating; this region is referred to as the thermo-mechanically affected zone, or TMAZ.

Research has previously been done that sought to determine the effects of friction-stir processing on aluminum alloys [Refs. 11-13]. It was found that FSP did refine the grain structure of these materials. Samples prepared from the stirs zones of processed material exhibited high strain rate superplasticity in addition to improvements in static strength and ductility.

C. OBJECTIVES OF THIS RESEARCH

Shear textures in the thermomechanically-affected zone (TMAZ) have been reported in previous examination of transverse planes. While characteristic shear textures were observed, the apparent orientation of the shear plane generally did not coincide with the interface between the stir zone and the TMAZ. Nevertheless, grain flow patterns in the TMAZ were usually consistent with the rotation motion of the tool and suggest shearing on planes tangent to the stir zone / TMAZ interface. This lack of coincidence suggests that states of strain in the material are more complex than simple shear and, in order to use the process effectively, its effects on the material must be understood. The purpose of this study is to apply recently developed orientation imaging microscopy (OIM) methods to evaluate the influence of FSP on microstructure and microtexture of an as-cast NAB material, focusing mainly on longitudinal planes (with respect to tool motion).

Computer aided orientation imaging microscopy (OIM) methods associated with electron backscattering diffraction (EBSD), energy dispersive spectroscopy (EDS), and optical microscopy were employed through the course of this research. The use of OIM analysis allowed for grain size to be accurately determined in addition to lattice orientation and grain boundary disorientation. These data could then be combined with that gathered from transverse planes in order to obtain a more complete picture of what happens to the material as it is processed.

The first phases of this work involved sectioning a processed sample of NAB in such a fashion that a series of OIM scans could be run on transverse planes progressing through the stir zone. The OIM was used in order to distinguish phases in the sample as well as to resolve features such as grain size and to determine grain-to-grain disorientations. The change of grain size and shape of the Cu matrix as well as the effects of FSP on the lattice orientation were of particular concern. This type of analysis was performed on a total of six planes ranging in position from base metal to TMAZ to the center of the stir zone back into base metal. An additional sample was prepared from the area of tool extraction in an attempt to determine the change in material properties ahead of the pin.

THIS PAGE INTENTIONALLY LEFT BLANK

II. BACKGROUND

A. COPPER-ALUMINUM SYSTEM AND DEVELOPMENT OF NICKEL-ALUMINUM BRONZE

Copper has generally good corrosion resistance and is the basis for a wide variety of alloys. Those alloys containing aluminum form the basis for aluminum bronzes. Cu-Al alloys containing less than 7 wt% Al solidify as a single-phase face-centered cubic (fcc) solid solution, denoted the alpha phase, and remain in this condition after being cooled to room temperature. Alloys with more than 9.4 wt% Al cool into a single-phase body-centered cubic (bcc) solid solution denoted the beta phase. If the beta phase is allowed to cool slowly alpha will form from the beta. Additionally, any untransformed beta phase undergoes a eutectoid reaction near 570°C thereby producing alpha + gamma.

The formation of gamma is undesirable because the high Al content causes the gamma phase to be anodic to the alpha phase [Refs. 9,14]. This may lead to dealuminization, which is similar in nature to the dezincification of brass. Nevertheless, high aluminum content is desirable from the point of view of strength and so steps are taken to minimize the formation of the gamma. This also results in alloys that are, overall, stronger and more ductile. [Refs. 9,14]. For the materials of the present study, this is accomplished by nickel and iron alloy additions.

Nickel and iron have been found to extend the alpha phase field and permit the use of a higher wt % of Al

without the formation of the gamma phase [Refs. 9,15]. This is illustrated in Figure 2.1, which combines the Cu-Al-Ni, Cu-Al-Fe and Al-Ni-Fe ternary diagrams for 500°C to show that the Ni and Fe additions result in the substitution of various Ni- or Fe- containing kappa phases in place of the gamma. Furthermore, NAB mechanical properties can be greatly improved via the addition of Ni and Fe.

By increasing the Al content of NAB alloys to 8.8 - 10 wt. % a material with increased strength, hardness and corrosion resistance can be created [Ref. 15]. The main drawback of the increase in alloying Al is a decrease in tensile elongation. The increased content of the lamellar kappa_{III} phase has been cited as the cause of this trend [Ref. 15]. The most desirable combination of properties for propellers are obtained from materials containing 9.5 wt. % Al when combined with 5 wt. % nickel, 4 wt. % iron, and 0.5 wt. % manganese.

Increasing the Fe content to 3 wt. % has been observed to cause a reduction in grain size and constrain grain growth at high temperatures, along with a reduction in the solidification range [Ref. 15]. Compositions containing from 3 - 5 wt. % Fe exhibit an increase in high temperature strength and strength retention [Ref. 15]. They also have improved wear and abrasion resistance and a notable increase in fatigue endurance limits [Ref. 15]. An optimum value of 4 wt. % Fe results in the best combination of properties [Ref. 15].

Nickel additions ranging from 0 - 5 wt. % Ni results in a grain refinement similar to that observed via the

addition of iron in addition to increased hardness and strength [Ref. 15]. The beta phase transformation is also slowed by the addition of this element [Ref. 15]. It should be noted that a severe attack on the second-phases in NABs may result from allowing the iron content of the material to exceed that of nickel [Ref. 15]. In order to maximize corrosion resistance the nickel content should ideally be 5 wt. % with a complimentary iron content of 4 wt. % [Ref. 15].

B. PHASES IN CAST NAB

NAB is thus a copper-base quaternary alloy with a composition as given in Table 2.1. Due to a nominal 9 wt. % content of Al as-cast nickel-aluminum bronze first solidifies as the BCC beta mentioned in the discussion of the Cu-Al alloy system. Further cooling of this beta phase results in decomposition of the beta to produce the four distinct phases of NAB; an FCC alpha matrix and three Kappa phases, designated $kappa_{II}$, $kappa_{III}$, and $kappa_{IV}$. A $kappa_{I}$ phase only forms in alloys containing more than 5 wt. % Fe. These kappa phases have been classified according to their individual morphologies as observed through optical microscopy, as well as according to the sequence in which they form. The phases will be explained in the order in which they form from the beta phase. These phases are shown in Figure 2.2a, a micrograph of as-cast NAB.

	Cu	Al	Ni	Fe	Mn	Si	Pb
min-max	min 79.0	8.5-9.5	4.0-5.0	3.5-4.5	0.8-1.5	max 0.10	max 0.03
nominal	81	9	5	4	1	-	-

Table 2.1: Chemical composition percent by weight of typical nickel-aluminum bronze. (Ref. 2)

1. Alpha Phase

The alpha phase represents an equilibrium solid solution or matrix with a fcc crystal structure. It has a lattice parameter a_0 = 3.64 angstroms. Alpha forms in the vicinity of 1030^{o}C from beta as a proeutectoid and often displays as a Widmanstätten morphology at moderate rates of cooling from the beta phase, which is consistent with the casting of components such as propellers. Alpha can occur intergranularly or intragranularly but slower cooled NAB consists of primarily intragranular alpha. The alpha phase can be seen as the light green phase in Figure 2.2a.

2. Kappa$_{II}$ Phase

There are four Kappa phases that may form in cast NAB: the kappa$_I$ phase, the kappa$_{II}$ phase, the kappa$_{III}$ phase, and the kappa$_{IV}$. The kappa$_I$ phase has the same composition and crystal structure as the kappa$_{II}$, but is coarser due to its formation at higher temperatures in high Fe content alloys. Because of this it is commonly accepted that there exists only a kappa$_I$ phase, which varies in size, versus the two distinct phases.

The kappa$_{II}$ phase is a globular, dendritic (rosette-shaped) structure found in NAB alloys containing less than 5 wt. % iron and ranges in particle size from 5 to 10 micrometers. It corresponds to an iron rich Fe_3Al composition. The kappa$_{II}$ phase has a DO_3 crystal structure with a lattice parameter, a_0, equaling 5.71 angstroms. The DO_3 structure is an ordered bcc superlattice consisting of eight cubic cells (Figure 2.2b). The kappa$_{II}$ phase forms from beta along with the alpha phase beginning at 930^{o}C and

is located near the lamellar eutectoid region of the microstructure. An NAB phase diagram and corresponding phase transformation diagram is represented in Figure 2.3.

3. $Kappa_{IV}$ Phase

$Kappa_{IV}$ is a fine cuboidal, cruciform precipitate formed within the alpha matrix beginning 850^{o}C. $Kappa_{IV}$ particles are of the same Fe_3Al composition and DO_3 crystal structure as the $kappa_{II}$ phase. The lattice parameter for the $kappa_{IV}$ phase is 5.77 angstroms vice the 5.71 angstroms for $kappa_{II}$.

4. $Kappa_{III}$

The $kappa_{III}$ phase represents a fine lamellar eutectoid with a NiAl chemical composition. $Kappa_{III}$ has a B2 crystal structure with a lattice parameter, a = 2.88 angstroms (approximately half that of $kappa_{II}$ and $kappa_{IV}$. The B2 structure for NiAl is an ordered CsCl crystal structure, which is hypothesized to form from $kappa_{II}$ particles that may act as a substrate for $kappa_{III}$ growth [Ref 17]. $Kappa_{III}$ forms at 800^{o}C and proeutectoid $kappa_{III}$ can be globular in morphology.

The casting of NAB structures may give varied microstructures within castings due to variation in local cooling rates that also give varying material properties. Overall slow cooling rates result in relatively weak as well as heterogeneous microstructures and, in addition, porosity, which further degrades material properties. These factors ultimately lead to material with lower strength and decrease its cavitation and corrosion

resistances. Additionally, poor control of the composition of NAB structures leads to inconsistent microstructures.

Propellers experience severe environmental conditions and stresses throughout their service life. Normal operating conditions expose propellers to a variety of destructive forces including cavitation, corrosion, and stresses that may be increased due to eroded/corroded surfaces. Large impulsive stresses may arise due to impact with objects and debris in the water. For these reasons it is apparent that eliminating the inherent defects that arise in casting without significantly altering the fabrication process will be of significant value. In so doing material the material properties are actually improved thereby extending the service lives of propellers. FSP offers that prospect of accomplishing these goals by improving the properties of cast NAB materials.

C. FRICTION STIR PROCESSING

The Welding Institute developed and patented friction stir welding (FSW) in 1991 [Ref. 8]. Friction-stir processing (FSP) is an offshoot of the technology used for friction-stir welding. Instead of joining two materials as is done in friction-stir welding, friction-stir processing is performed on a single piece of material for the purpose of microstructure modification. The “stirring” motion caused by friction between the tool and the material homogenizes and refines the material’s microstructure.

FSP uses a non-consumable tool in what is essentially a modified milling machine in order to process the material. The tool is usually fabricated from a heat

treated tool steel and consists of a cylindrical shoulder with a smaller diameter concentric pin. The pin can be a variety of shapes and is plunged into the material while being rotated until the shoulder engages the material surface, as seen in Figure 2.4. The workpiece material must be clamped to avoid excessive movement. Once engaged, the tool is then traversed across the material surface. This can be done in a single pass or in multiple passes. The shape and size of shoulder of the tool in addition to the length of the pin control the depth of surface penetration. The rotating tool creates plastic deformation and adiabatic heating mainly through sticking friction. The shoulder of the tool prevents upward flow of the metal that is being physically displaced by the pin, and forges the heated material. Tool shoulder diameters are typically about 25 mm, with pin diameters between 6 and 10 mm, and pin depths ranging from 6 to 12 mm. FSP uses sticking friction, although a small amount of slipping friction is present, and large plastic deformations in order to produce controlled adiabatic heating of the material. The heating causes the material to soften but is not sufficient to melt it, so that FSP is a solid state process. A typical temperature distribution created by tool rotation is seen in Figure 2.5 [Ref 27]. FSP causes such large deformation that material can move from on side of the tool to the other. A processed NAB sample consists of three distinct regions: stir zone/nugget, the thermo-mechanically affected zone, and base metal. This is illustrated in Figure 2.6.

The stir zone, also called the nugget, is the region most highly affected by the friction-stir process. Intense plastic deformation and a resultant fine-grained, defect

free microstructure are the benefit of the process. The grain size in the stir zone may be refined to a value of 3 micrometers [Ref. 7]. Tensile tests of specimens fabricated from the stir zone of NAB materials processed by FSP have shown a doubling of the nominal material yield strength coupled with an approximate 66% increase in ultimate tensile strength (Figure 2.7a). A significant increase in ductility was also noted. The stir zone and TMAZ are also harder than the original base metal (Figure 2.7b). In nickel-aluminum bronze this region may comprise of fine, equiaxed grains as well as Widmanstätten structures, and banitic or martensitic transformation products. A region of severe plasticity and heating effects lies beneath the stir zone and is identified as the thermo-mechanically affected zone (TMAZ).

The TMAZ is similar to the heat-affected zone (HAZ) that exists in conventional fusion welding. The TMAZ is characterized by significant plastic deformations although much less severe than in the stir zone, coupled with heating effects created by the rotating tool. Therefore, the TMAZ experiences steep strain and temperature gradients in a short distance (200 - 400 micrometers). The combination of these effects results in the development of shear textures within the TMAZ. Shear textures stem from slip by dislocation motion under conditions of nominally pure shear deformation. The deformation would correspond to conditions dominated by strain hardening and recovery. The deformed grains would contain recovered subgrain structures that exhibit a continuous increase in misorientation during deformation under such conditions [Ref. 7]. Friction stir welded aluminum and magnesium

materials developed shear textures that reflect an alignment of the shear plane in the texture as the tangent to the TMAZ/stir zone interface everywhere around the stir zone [Ref. 19]. Understanding shear textures is important in that it provides insight into the stresses and strains the metal experiences in this region. The modeling of this process must predict these stress and strain states for individual materials. The ultimate goal is to create an accurate computer simulation of the process. Previous work suggests that the shear textures developed in the TMAZ will often be of the C type when measured in the transverse plane. Canova et al [Ref. 20] had given the classification of shear textures. Grain structure within the TMAZ consists of large but distorted grains when compared to the grains in the stir zone. However, the TMAZ still exhibits improved material properties over the parent material.

The bulk of the material remains as base metal and is relatively unaffected by processing with the exception of minor heating effects near the base metal/TMAZ interface. Base metal exhibits the same microstructure and material properties as the as cast material, including defects.

The microstructure of friction-stir processed NAB is not uniform. Grain sizes vary throughout the regions themselves in addition to the obvious differences from region to region. This may be attributed to many factors including tool rotation speed and translation rate leading to inconsistent peak temperatures and exposure times to them [Ref 7]. Although varied, all processed microstructures exhibit material properties that are superior to those of the parent metal.

FSP produces localized microstructural changes thereby enabling the freedom to process selected areas of an object. Processing the material does not generate fumes, is not hazardous to the environment and requires no special precautions. Additionally no special material preparation is required prior to processing. Cost is reduced due to the use of a tool that is reusable; thus, the process can be performed in numerous environments, is safe, and is cost effective.

Friction-Stir represents a major advance in material processing. In order for it to be used in large-scale production the process and it underlying physics must be properly understood. This research is meant to enable that. Computer modeling/simulation of the friction-stir process for nickel-aluminum bronze requires extensive experimentation and patience, but is of possible great benefit to society and the United States Navy.

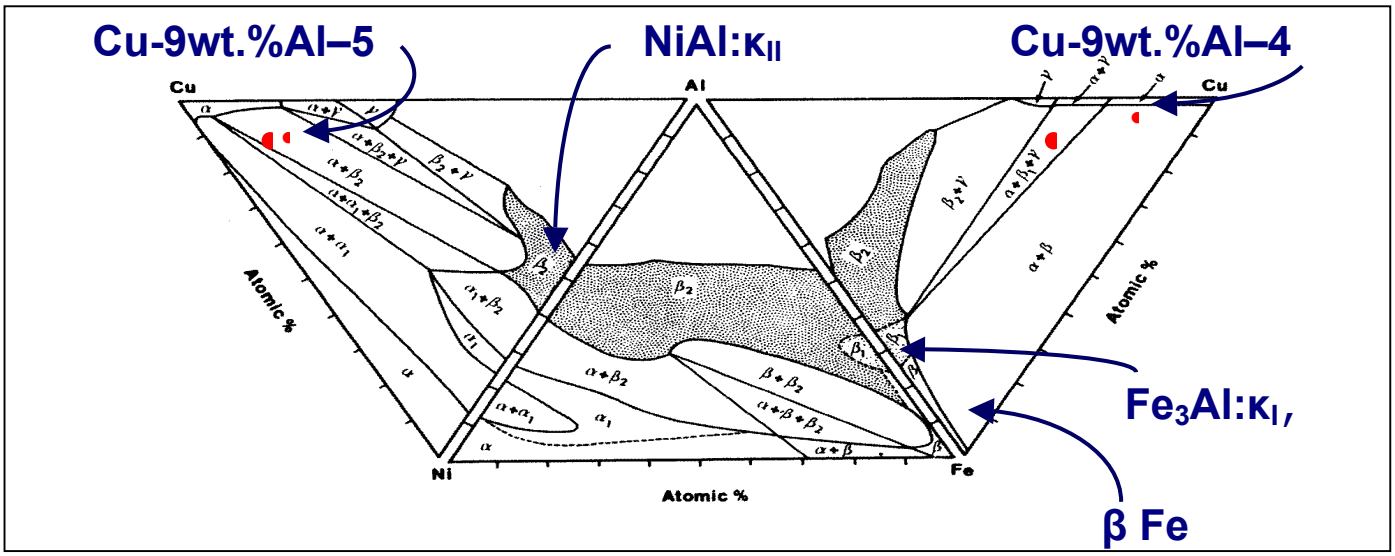

Figure 2.1: Quaternary equilibrium NAB phase diagram. F. Hasan, A. Jahanafrooz, G.W. Lorimer and N. Ridley, Metall. Trans. A., vol. 13A (1982) pp. 1337-45. (Modified courtesy T. R. McNelley.)

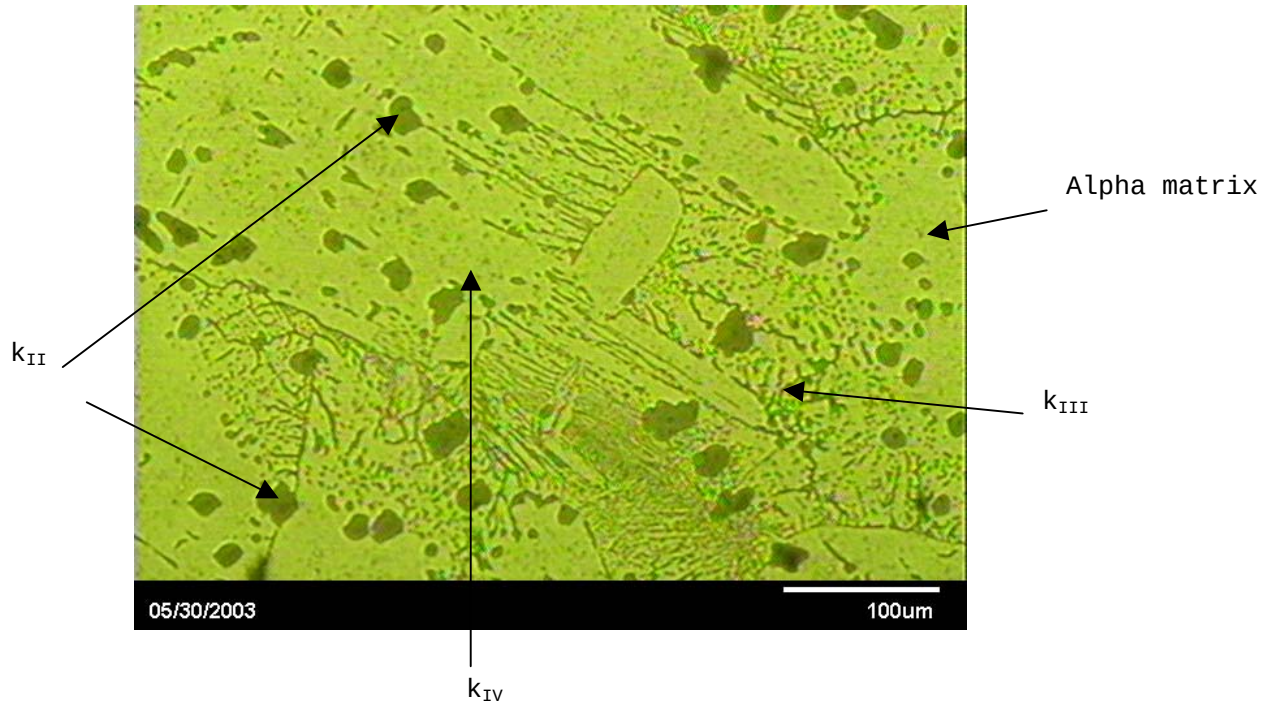

Figure 2.2a: Optical micrograph of as-cast NAB at 370x. $kappa_{II}$ is the globular, dendritic structure, $kappa_{IV}$ is the very fine particulate imbedded with in the alpha matrix (surrounding light green phase), $kappa_{III}$ is the lamellar "finger-like" structure (image courtesy of William Nabach).

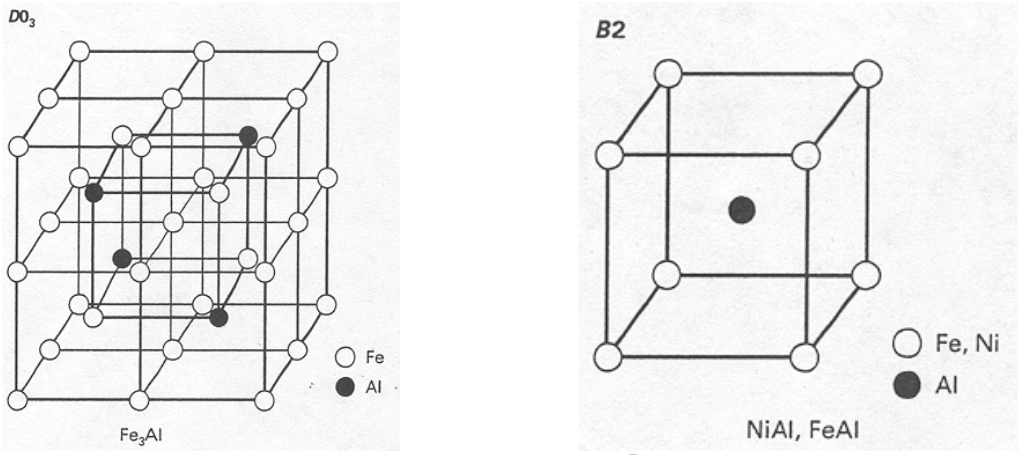

Figure 2.2b: DO_3 and B_2 crystal structures. $Kappa_{II}$ and $kappa_{IV}$ have a Fe_3Al composition with a $D0_3$ crystal structure, while $kappa_{III}$ exhibits a NiAl composition with a B_2 crystal structure.

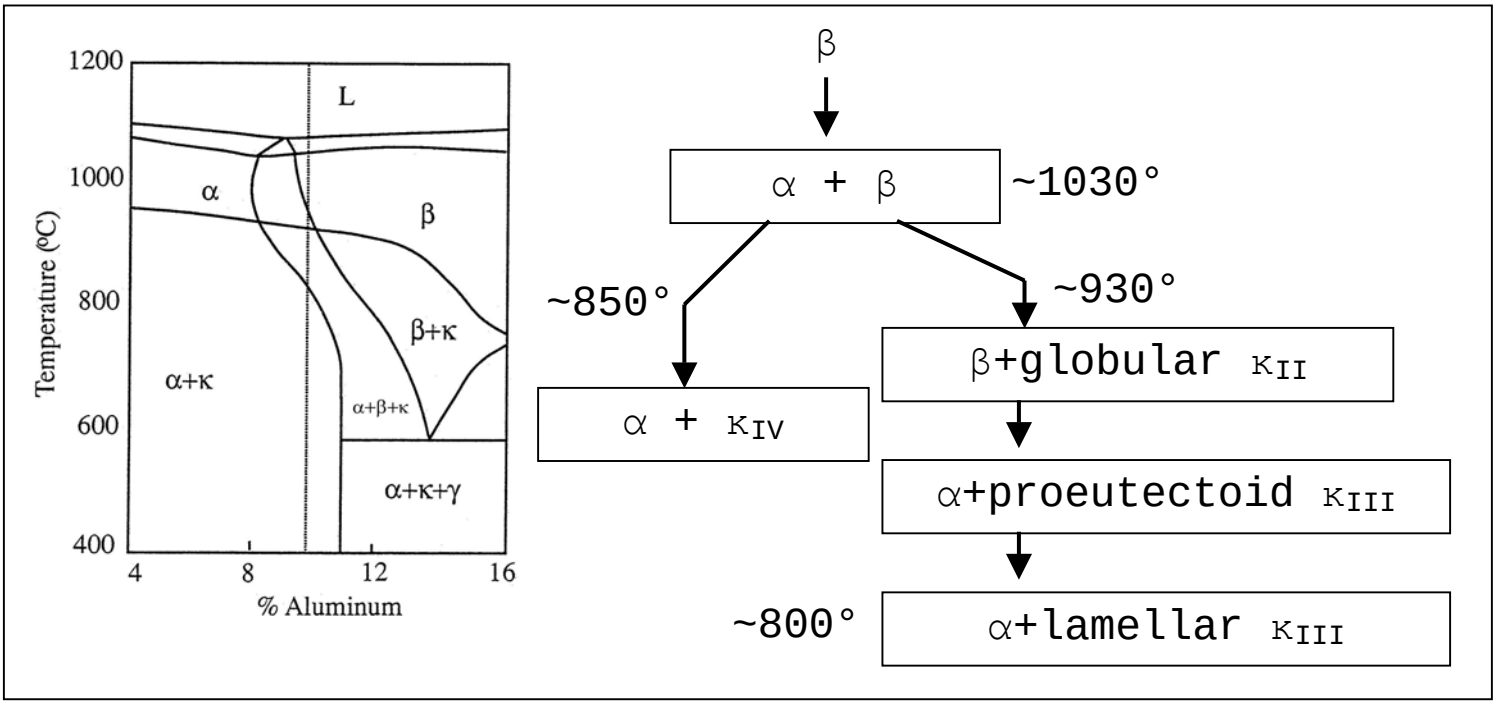

Figure 2.3: NAB phase diagram with corresponding transformation diagram (image courtesy of William Nabach)

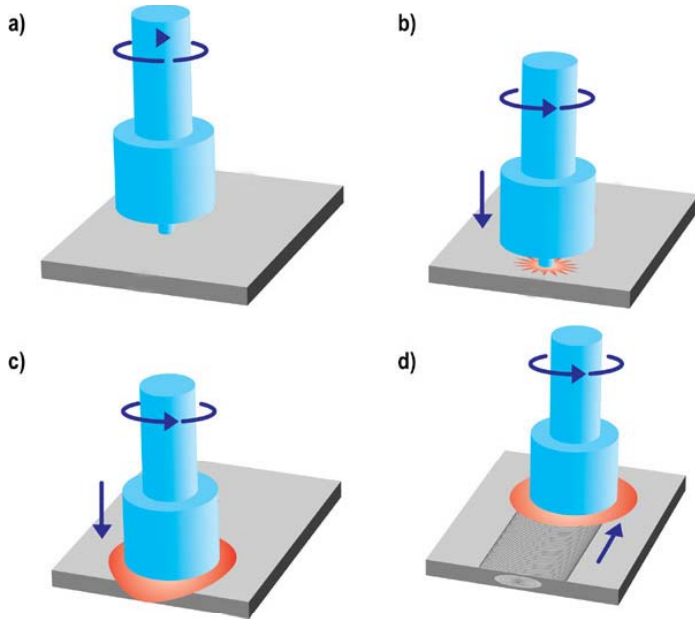

Figure 2.4: Friction Stir Process. A rotating tool a) is plunged into the material surface b). Once engaged up to the shoulder c) the tool is traversed across the material surface d). FSP is not a superficial process, affecting material well below the pin depth. The advancing side is that in which tool rotation and tool translation are in the same direction. On the retreating side tool rotation is opposite tool translation.

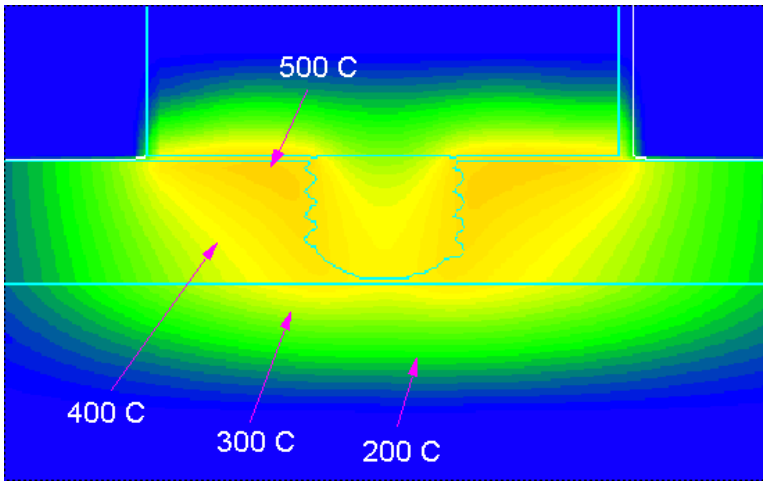

Figure 2.5: Temperature distribution in FSP. Temperatures have been known to reach upwards of 850°C. A. Askari, Boeing INC, Private Communication (June 2003).

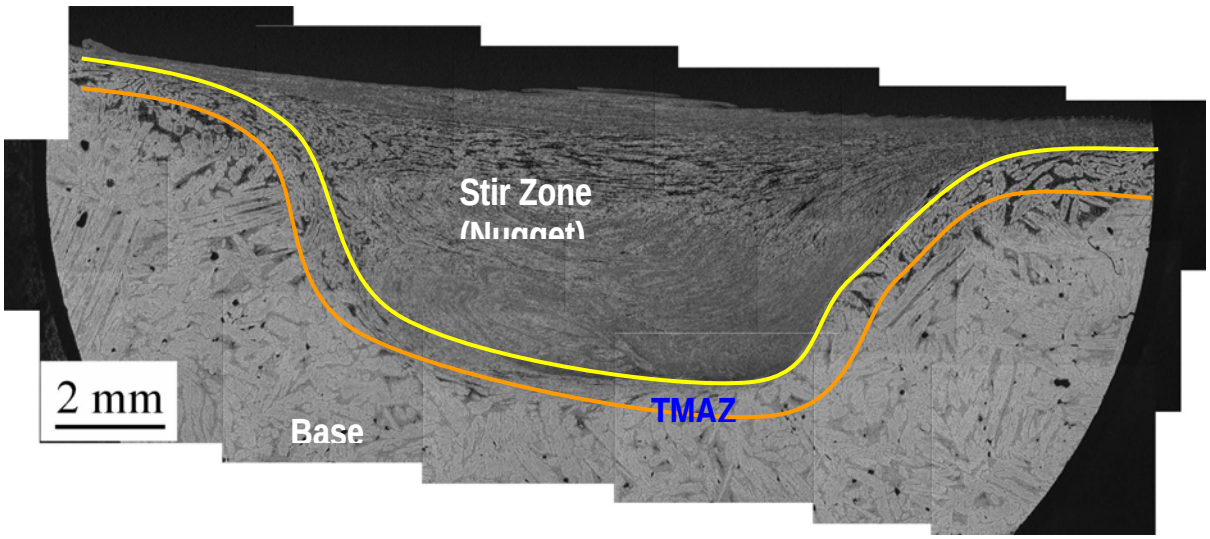

Figure 2.6: Regions resulting from FSP in 576 condition. The stir zone is characterized by extensive plastic deformation as induced by the rotating tool. The TMAZ experiences both large plastic deformations and heating effects. Base metal remains relatively unchanged from the as-cast condition, experiencing minute deformations and heating effects.

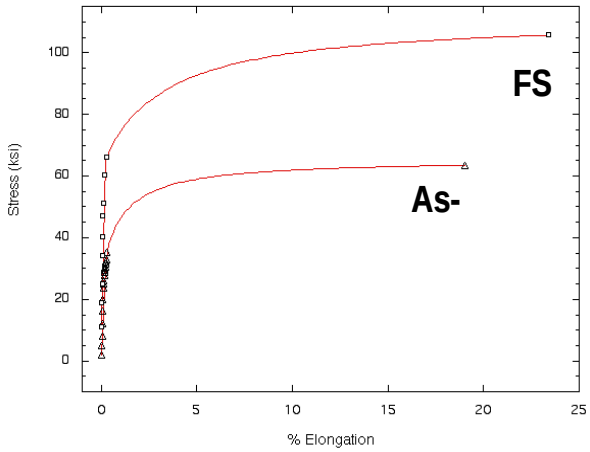

	Yield Strength (ksi)	Tensile Strength (ksi)
FSP	62.8	107.8
As-cast	31.2	64.8

Figure 2.7a: Stress vs strain plot for FSP vs as-cast NAB tensile samples (data and graph courtesy of M. Mahoney).

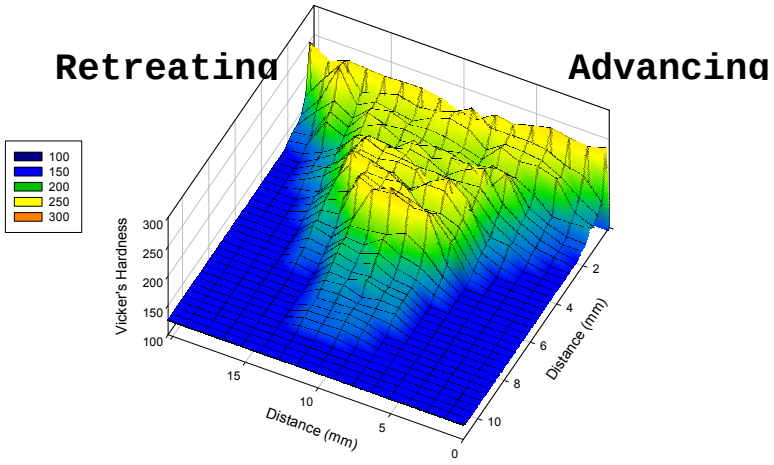

Figure 2.7b: Hardness variation in friction-stir processed NAB. Note large hardness increase in stir zone.

III. EXPERIMENTAL PROCEDURES

A. SAMPLE PREPARATION

An cast nickel-aluminum bronze (NAB) plate 77.2 mm wide, 7 mm in thickness, and approximately 300 mm in length that had been subjected to FSP was provide by Rockwell Scientific Corp. the sample is shown in Figure 3.1. The FSP procedure was designated 676 and processing was conducted using 800 rpm and 6 inches per minute traversing speed. This is designated here as 676 800/6. The sample was then cut twice perpendicular to the tool travel direction. This yielded three sections, the middle section being used for the experimentation involved here. It measured 77.2 mm by 32 mm by 7 mm. The sample was then cut in a direction parallel to tool travel in such a manner that thirteen approximately equal sections were created. This is illustrated Figure 3.2. An additional sample equivalent to sample 7 with the exception that it included the void created from withdrawal of the tool is depicted in Figure 3.3.

Figure 3.1 Original Sample

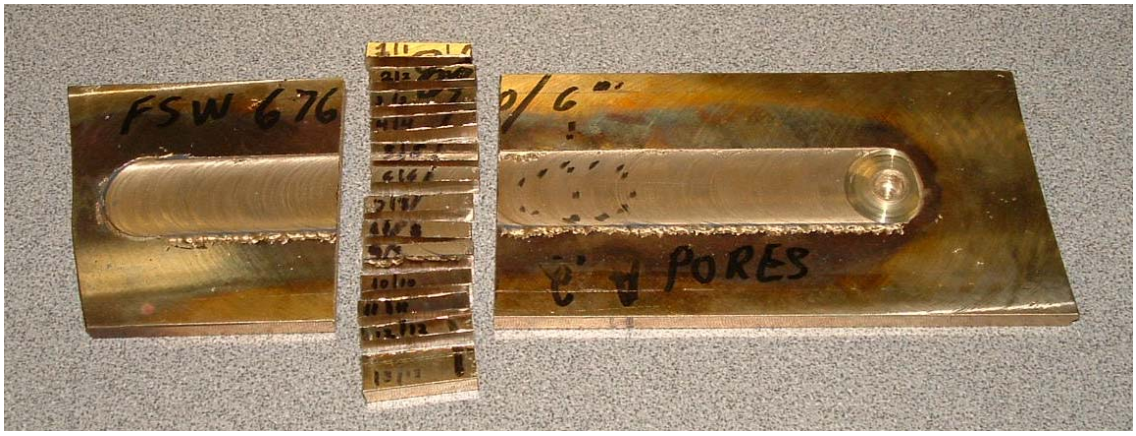

Figure 3.2 Sectioned Sample

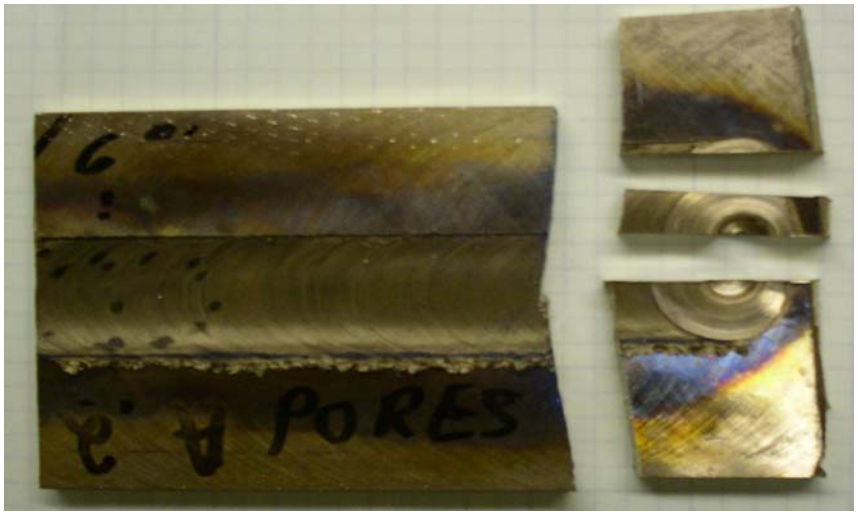

Figure 3.3 Tool Front Sample

Mechanical polishing of the samples was accomplished following the steps outlined in Table 3.1 for the indicated times. Water was used as a lubricant for the silicon carbide (SiC) paper. Grinding was done in one direction for approximately ten seconds and the sample was then

rotated 90^{o}. This process was repeated until all evidence of prior grinding was eliminated. Grinding on SiC paper was done with a downward pressure of approximately 20 N. Final polishing was done with Al_2O_3 using a downward pressure of approximately 1 N. The pressure used with the Al_2O_3 was significantly lighter than that used with the paper. It was noted that the heavier pressure with the paper led to a quicker polish with a level of quality equal to that created with a lighter pressure. However, once the sample was to the Al_2O_3 stages it was noted that heavy pressures led to numerous problems. These included: tearing out of the kappa phase particles, grooves worn into the sample, and isolated gouges (caused by the passing of torn-out particles across the sample surface. Additionally, after each mechanical polishing step, the sample was thoroughly rinsed with distilled water and ethanol. One should note that the polishing process occasionally requires more than one repetition in order to obtain a suitable finish.

Step	Abrasive	Time	RPM
1	800 Grit SiC paper	1 min	n/a
2	2400 Grit SiC paper	1 min	n/a
3	4000 Grit SiC paper	3 min	n/a
4	1 micrometer Al_2O_3	20 min	120
5	0.05 micrometer Al_2O_3	45 min	80

Table 3.1 Polishing Grits and Times

A finish with a small nominal surface flaw size was needed because of the small interaction volume of the electrons at the surface of the sample. In order to ensure proper imaging in the SEM electropolishing was found necessary. This was conducted at 30 volts for 10 seconds in a Buehler Electromet 4. The solution used was a 33% Nitric Acid-66% Ethanol electrolyte solution cooled to 3°C.

B. OPTICAL MICROSCOPY

Optical microscopy of the as-cast and FSP NAB samples was conducted with a JENAPHOT 2000 Reflected-Light photomicroscope, equipped with a SEMICAPS Genie SEM digital imaging system.

C. ORIENTATION IMAGING MICROSCOPY (OIM)/ELECTRON BACKSCATTER PATTERN (EBSP) COLLECTION AND ANALYSIS

A TOPCON SM-510 Scanning Electron Microscope (SEM) with a tungsten filament was used with an accelerating voltage of 20KV. For the purposes of this research ten to twelve 100 x 100 micrometer scans were performed on every other sample with the addition of a few 200 x 50 micrometer scans performed in order to give a complete picture of microstructure variation. OIM collects data from diffraction patterns caused by scattered electrons called electron backscatter patterns (EBSPs). The as-electopolished samples were put into the SEM in an aluminum holder that held the sample surface at 70°, thereby allowing the collection of EBSPs from a phosphor screen, attached to a low light camera. With the OIM software, initial values of the material characteristics must be entered into the software in order to ensure that proper

indexing of the phases occurs during data collection. During scanning, the OIM software uses the electron beam of the SEM in order to traverse the surface in a raster-like pattern over the sample surface. For each point its location via Cartesian (x-y) coordinates, lattice orientation, image quality (IQ), confidence index (CI) and phase identification are recorded. Comparing the detected electron backscatter patterns with diffraction patterns that are calculated by the computer performs this process. The computer patterns are based on input parameters (i.e. lattice parameters and crystal structure). Detected patterns are then compared to the calculated patterns. The order that the calculated patterns were inputted is important in that the computer compares them in that precedence. If a satisfactory match cannot be made, the software defaults to the first input pattern on the list; otherwise, the data point is indexed to the phase that most nearly matches the detected EBSP. A confidence index is assigned to the data point; thus, the accuracy of the software in matching the detected phase with a calculated phase is indicated. The basic setup of the equipment is shown schematically in Figure 3.4.

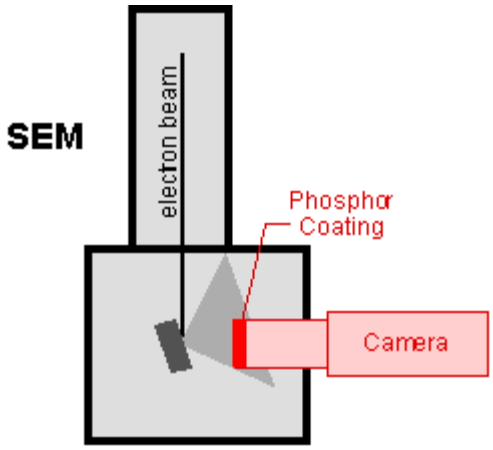

Figure 3.4 SEM Equipment Setup

External reference axes are necessary for OIM; these were defined as follows: the reference direction (RD) was assigned as positive downward; the normal direction (ND) was directed toward the phosphor screen, and transverse direction (TD) was parallel to the horizontal and corresponds to the toll travel direction. In this case, ND also represents the transverse direction with respect to the processing direction (i.e. processing direction was from left to right). Lattice orientations may then be defined in terms of Euler rotation angles that bring the cube axes of the lattice into coincidence with the reference axes. These axes are illustrated in Figure 3.5.

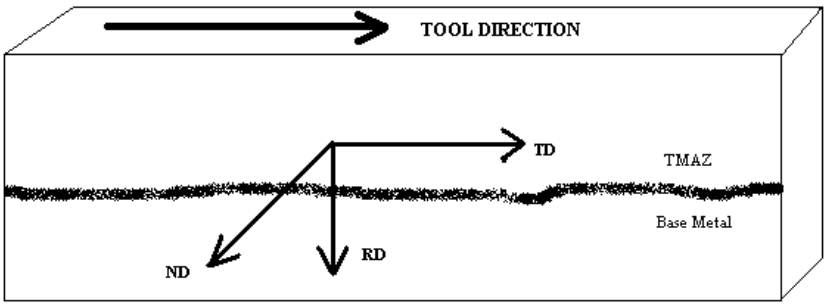

Figure 3.5 Sample Reference Axes

The electron beam from the SEM was operated in spot mode with a beam diameter less than 0.2 µm. This allowed the electrons to interact with the first 30-50 nm of the sample surface, undergoing Bragg diffraction. Diffracted electrons then impinged upon a phosphor screen, thereby illuminating it. A low light level camera was then used to capture the images from the phosphor screen. The OIM equipment was then used to analyze the pattern. Figure 3.6 illustrates a sample Kikuchi pattern and how the indexing is overlaid onto the image of the pattern.

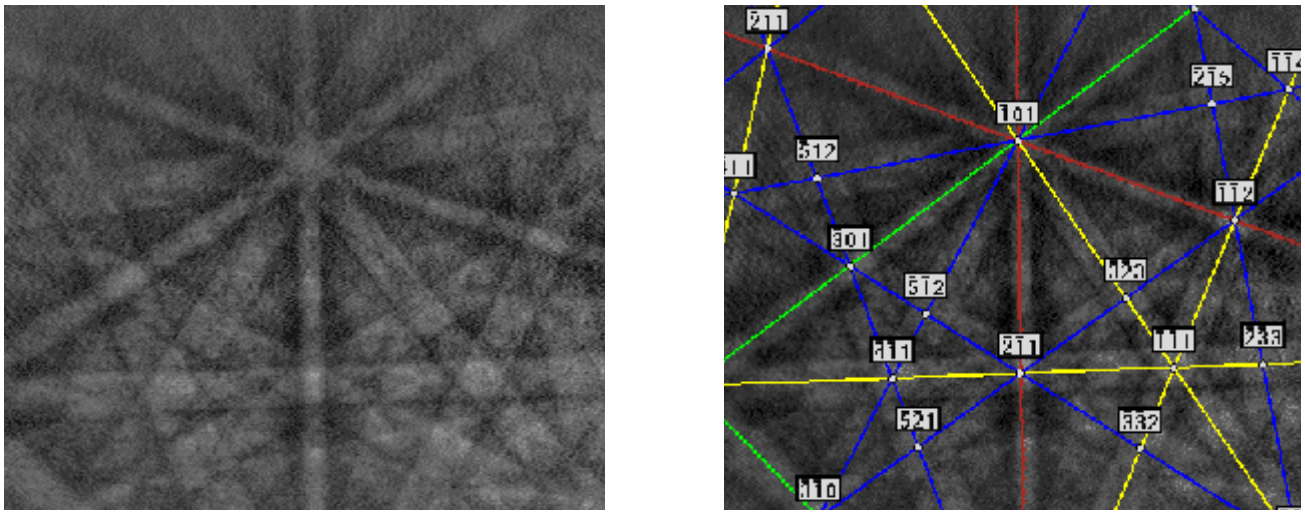

Figure 3.6 Sample Kikuchi Pattern and Index Overlay

Various combinations of these parameters may then be used to create visual representations of spatial distribution of, for example, crystallographic orientation, or image quality (IQ) of the diffraction images. Orientation data may be presented as grain orientation maps, pole figures, histograms of the grain-to-grain misorientation angles, etc. Here, misorientation angle refers to the minimum rotation angle among all crystallographically equivalent rotations that bring neighboring lattice orientations within the same phase into coincidence. Various data clean-up steps are performed and typically involve three successive steps. First, individual points that do not belong to any grains are assigned to match the neighboring majority grain. Second, the highest CI for a grain is assigned to all points in that grain. Third, data points with CI's less than 0.1 are compared to those of nearest neighbors and the neighbor with the highest CI is reassigned to that point, thus effectively making it a point in that grain. This clean-up step assumes that the low CI points are located near grain boundaries or areas of high dislocation density and that the point with the higher CI is the true orientation for the low CI point. It should be noted that any single point with a CI greater than 0.1 will not be altered by this procedure. Grains with good quality EBSP's, no matter what grain size, will be saved unchanged. The elimination of low CI points was done in order to obtain a true picture of the grain boundaries and the angular disorientation between grains. After the clean up procedure is completed, the OIM software is used to produce OIM grain maps, pole figures and rotation angle histograms, as described previously. Further discussion of

phase identification will be provided subsequently when the results of analysis of the as-cast and FSP NAB samples are presented. While it is possible to conduct OIM on multi-phase materials this area of the technique is less well developed than orientation determination and analysis.

THIS PAGE INTENTIONALLY LEFT BLANK

IV. RESULTS AND DISCUSSION

This chapter will discuss the application of Orientation Imaging Microscopy (OIM) to the analysis of shear textures in the TMAZ of friction-stir processed NAB. The shear textures (slip directions and lattice orientations) were observed using OIM techniques. The shear textures of focus will be those analyzed on the FSP 676 sample as discussed in the previous chapter.

A. ORIENTATION IMAGING MICROSCOPY

Orientation imaging microscopy has been utilized in order to identify phases and analyze textures in as-cast nickel-aluminum bronze. The OIM software used in this study is divided into two parts: a data collection program and a data analysis program. The data collection software [Ref 22] collects location, phase, lattice orientation, and measures of pattern quality and confidence in accuracy or orientation determination. The analysis software [Ref 23] analyzes and organizes the data to enable its display it in a presentable form.

Cuevas [Ref. 7] determined that OIM instruments were capable of analyzing multiphase alloys such as NAB, but may encounter difficulty distinguishing phases having cubic crystal structures with inter atom distances that differ only slightly (i.e., the B2 and DO3 structures present in NAB). Here, OIM data only for the alpha matrix were analyzed to determine textures within the TMAZ.

B. FSP 676 PRIMAY DATA

Using OIM longitudinal sections (3,5,7,9,11,13 and a sample sectioned through the hole left by the withdrawn pin) of the 676 condition were scanned (using the procedure and scanning pattern delineated chapter 3). Orientation data and image quality maps from these samples form the main basis for analysis of this material. Figure 4.1 shows the relative locations of the scans on a schematic diagram of a sample that applies to all samples except sample 7. Sample 7 had two columns of six evenly spaced scans, as opposed to the two columns of five scans depicted below. This enabled particular focus on the center of the stir zone. The images are organized with an image quality map on top of its corresponding orientation data. The images are aligned in columns in same manner as depicted by Figure 4.1. The rows of scans are labeled using lower case letters starting with the letter “a”, which denotes the topmost row. The observations were made with respect this data follows the last data set of each sample.

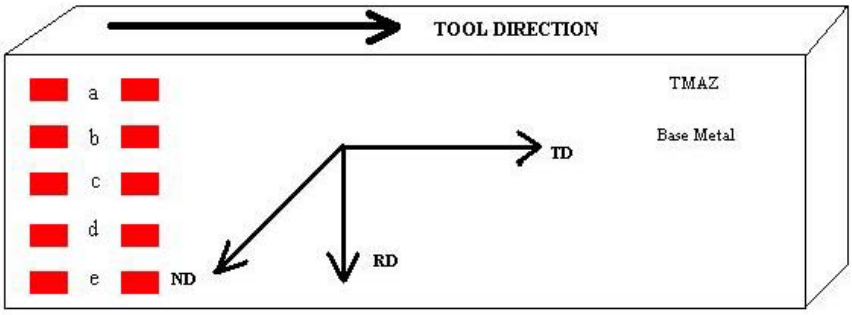

Figure 4.1 Generic illustration of scan locations. The spacing between the two columns is approximately 4mm on all samples.

Row a

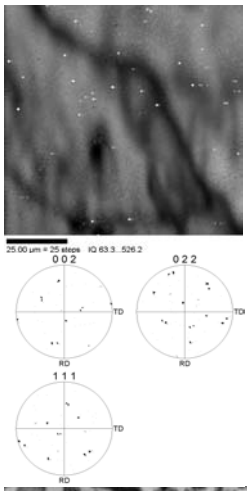

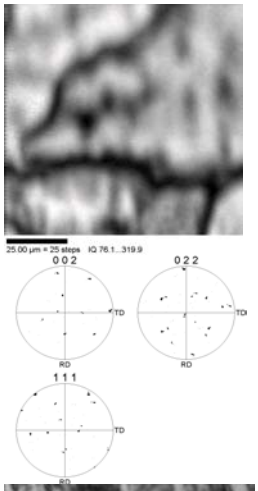

Row b

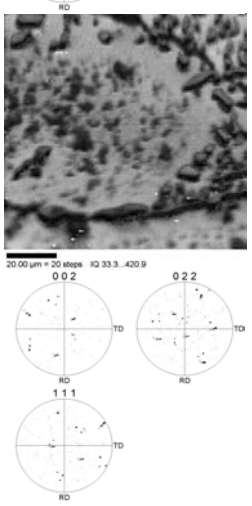

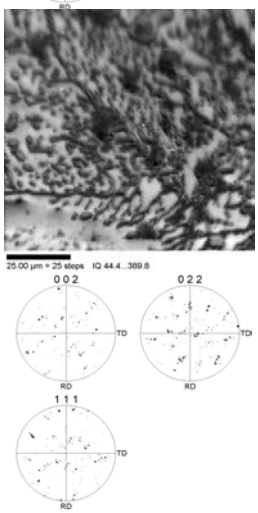

Figure 4.2 Sample 3 rows a and b

Row c

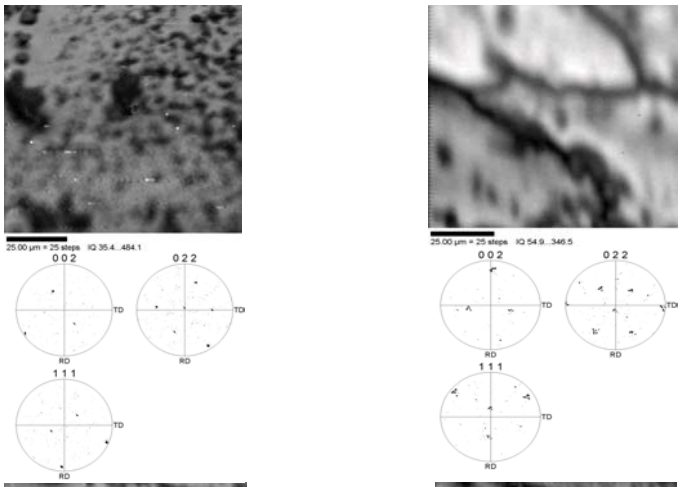

Row d

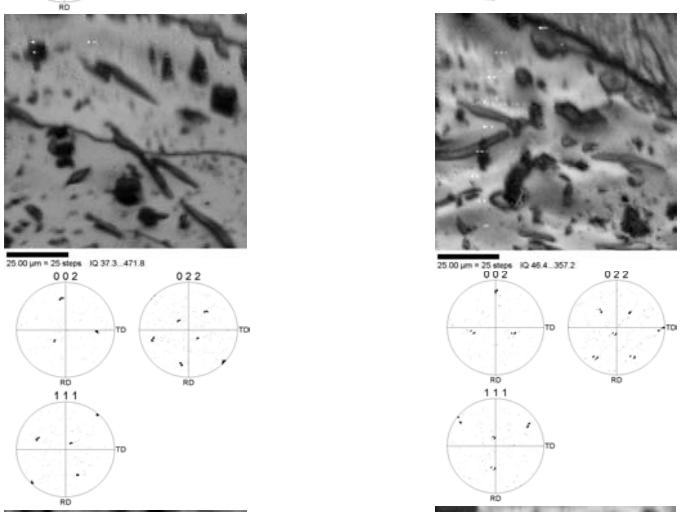

Row e

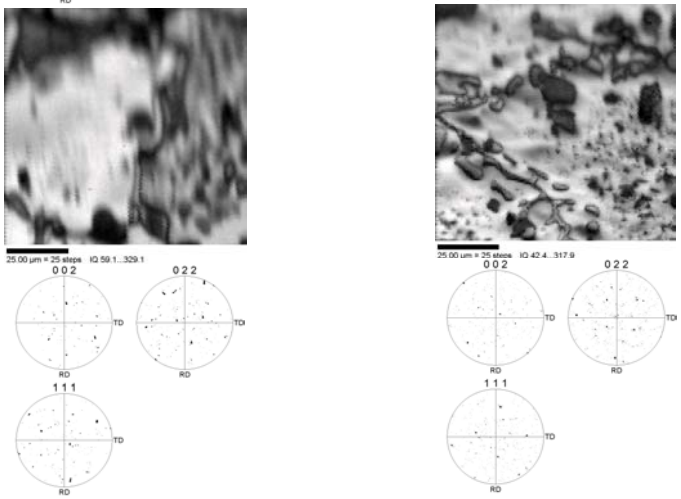

Figure 4.3 Sample 3 rows c through e

The material depicted here is base metal located on the retreating side of the tool. However, it should be

noted that some variation is evident along both the TD and RD directions.

Row a

Row b

Row c

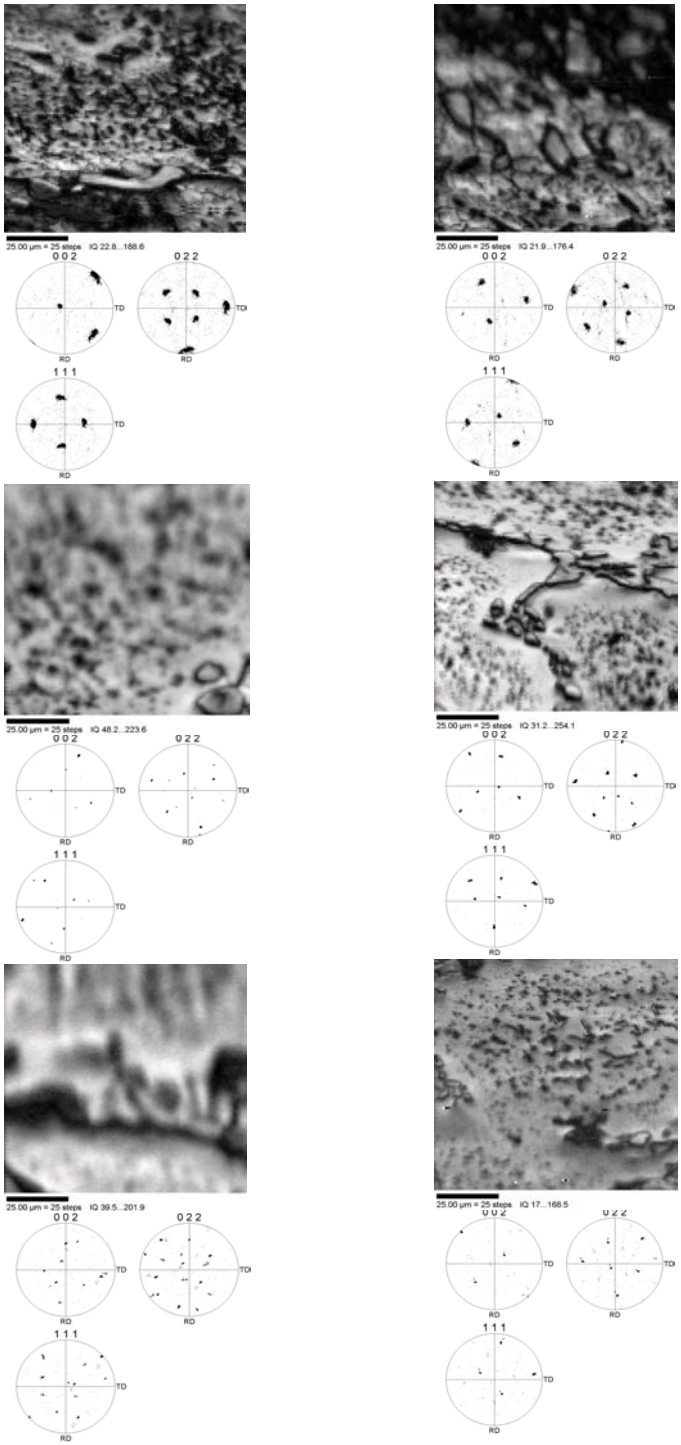

Figure 4.4 Sample 5 rows a through c

Row d

Row e

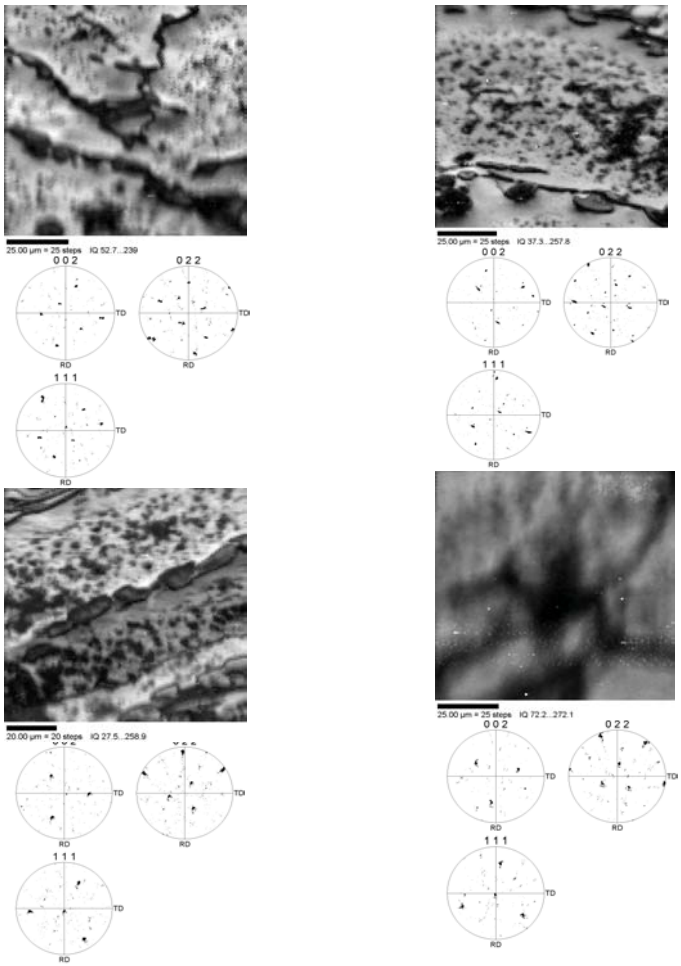

Figure 4.5 Sample 5 rows d and e

Row a of sample 5 is in the TMAZ on the retreating side of the tool. Despite a fine grain size it is apparent that a preferred orientation exists in this region. Additionally, the two scans in the row have a different orientation, as is evident in the orientation data. Rows b through e are all in the unaffected base metal and are similar to sample 3 in that no strong preference for an orientation is evident.

Row a

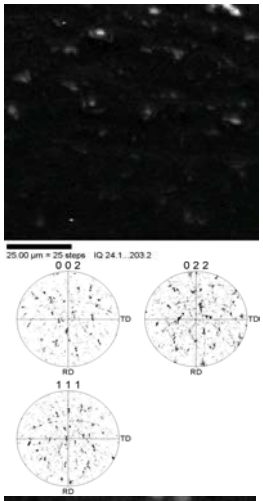

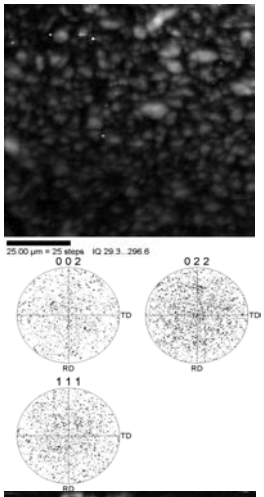

Row b

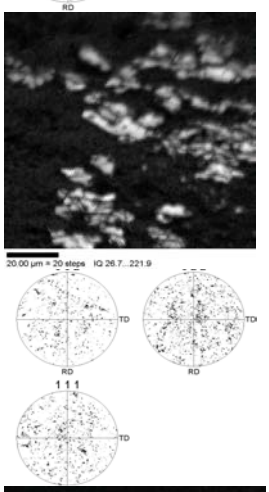

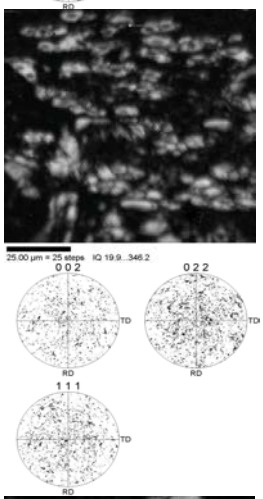

Row c

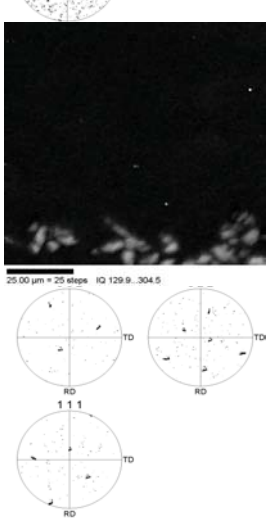

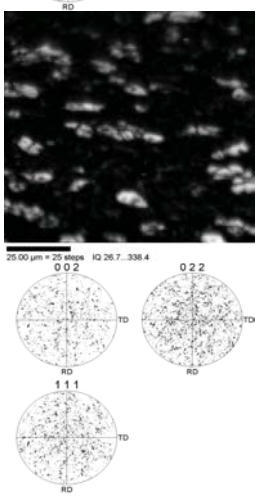

Figure 4.6 Sample 7 rows a through c

Row d

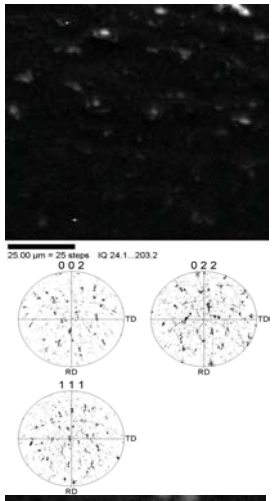

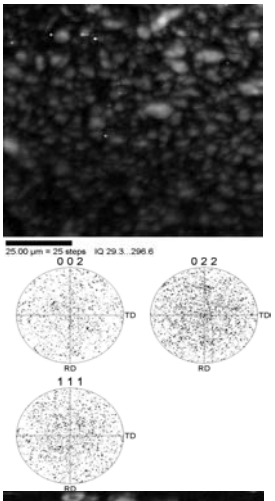

Row e

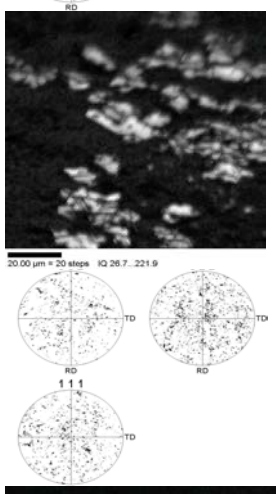

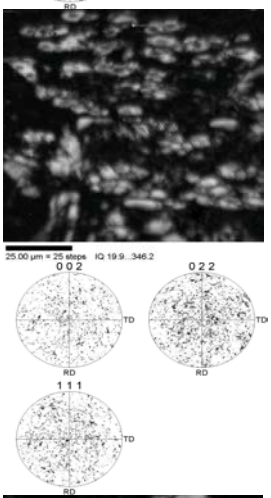

Row f

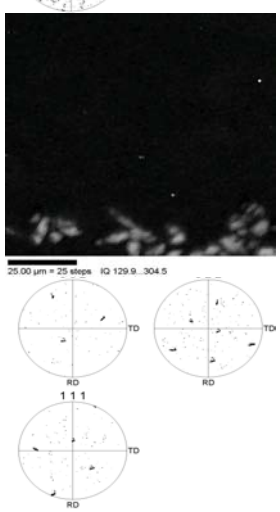

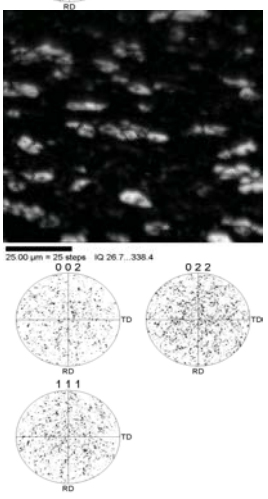

Figure 4.7 Sample 7 rows d through f

Sample 7 is located in the center of the nugget. The pole figures indicate that the orientations are random. A fine-grained microstructure is also evident in this area.. Altogether, these data indicate that the stir zone has experienced recrystallization during processing. It is likely that the presence of a particle dispersion coupled with the severe plastic deformation leads to particle stimulated nucleation [Ref.7] and development of a random distribution of grain orientations.

Row a

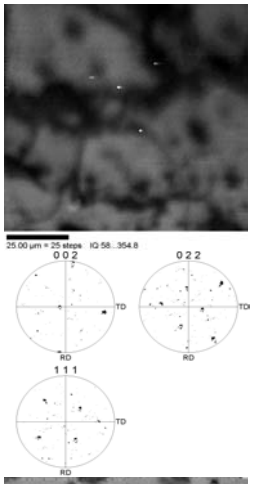

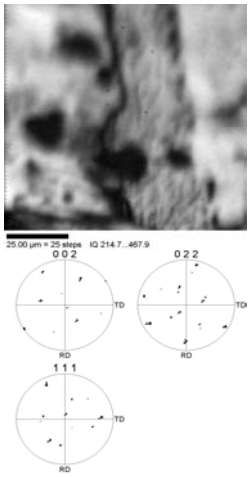

Row b

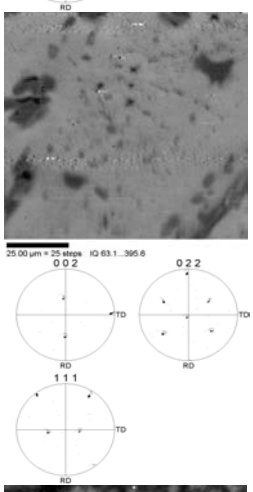

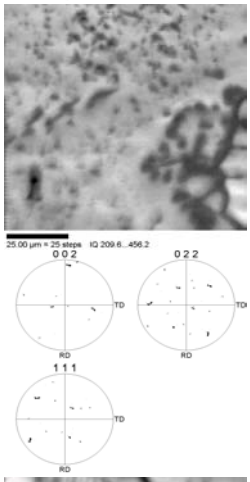

Row c

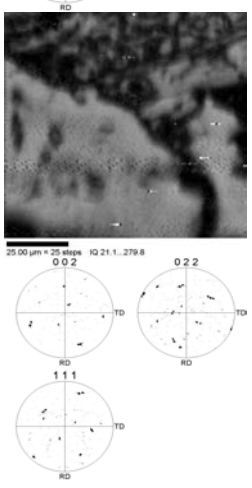

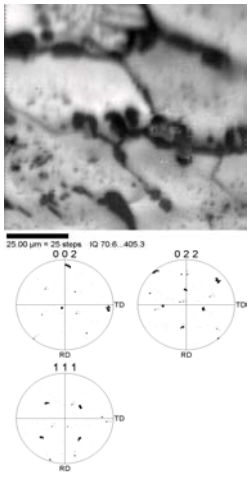

Figure 4.8 Sample 9 rows a through c

Row d

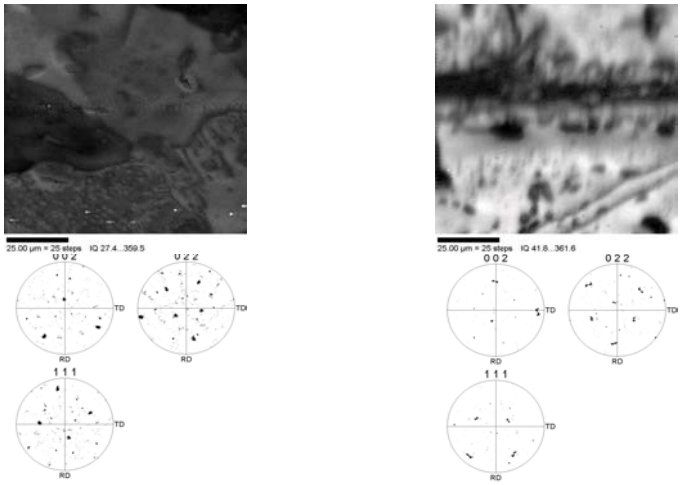

Row e

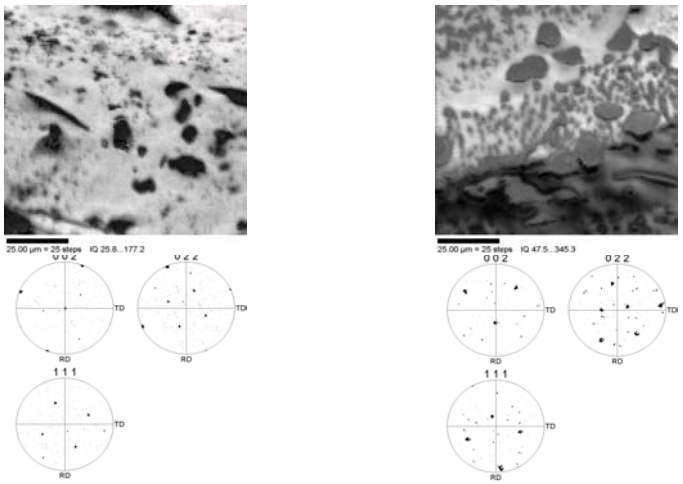

Figure 4.9 Sample 9 rows d and e

Sample 9 is located 10mm from the center of the stir zone on the advancing side. As was seen in Row a of sample 5 variation along the TD and RD is evident in all rows. Additionally, one should note that, similar to latter rows of sample 5, that no strong preference for an orientation is evident and it is likely that all areas represent base metal. This sharply contrasts Row

a of sample 5 in which a strong orientation is apparent in a fine-grain material.

Row a

Row b

Row c

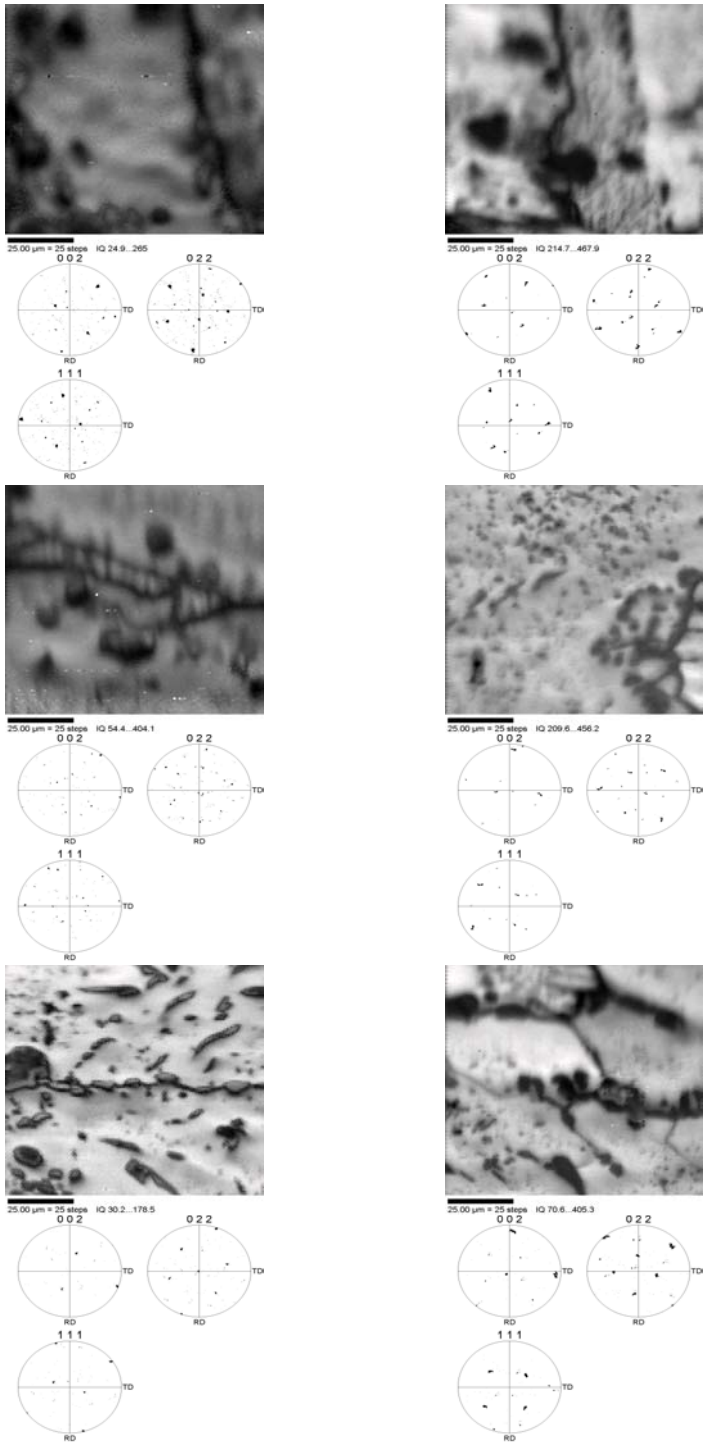

Figure 4.10 Sample 11 rows a through c

Row d

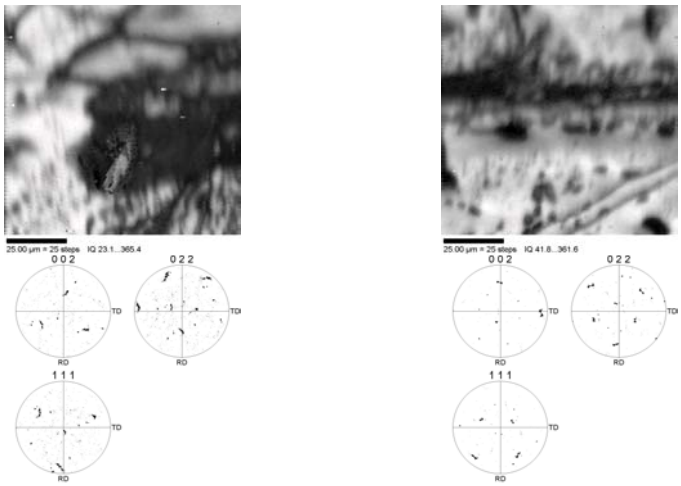

Row e

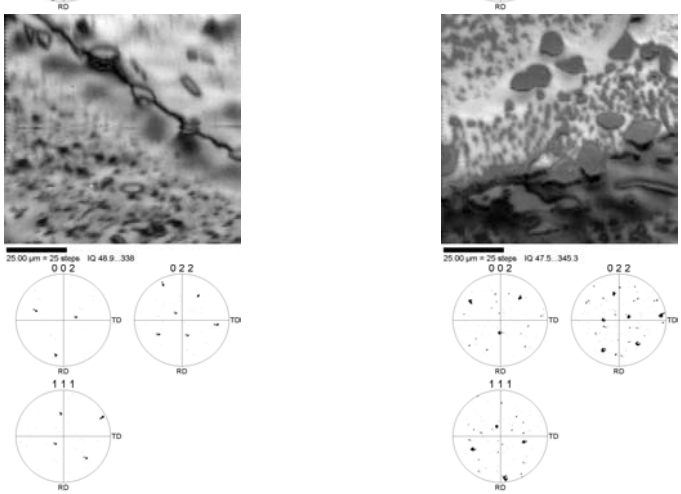

Figure 4.11 Sample 11 rows d and e

Sample 11 is located just outside the TMAZ on the advancing side. Variations along the TD and RD directions are evident throughout the collected data. This illustrates the variation that is evident in as-cast NAB.

Row a

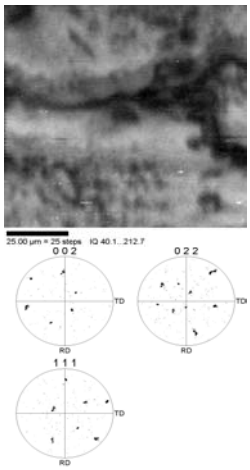

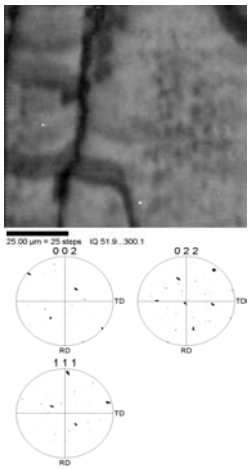

Row b

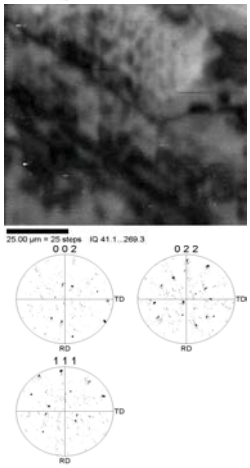

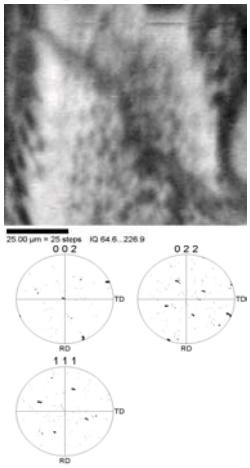

Row c

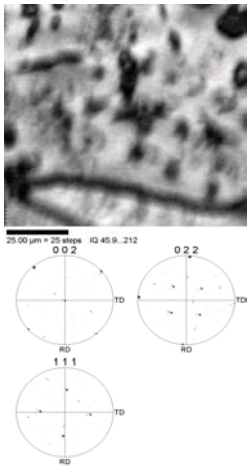

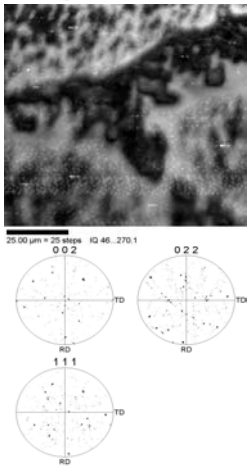

Figure 4.12 Sample 13 rows a through c

Row d

Row e

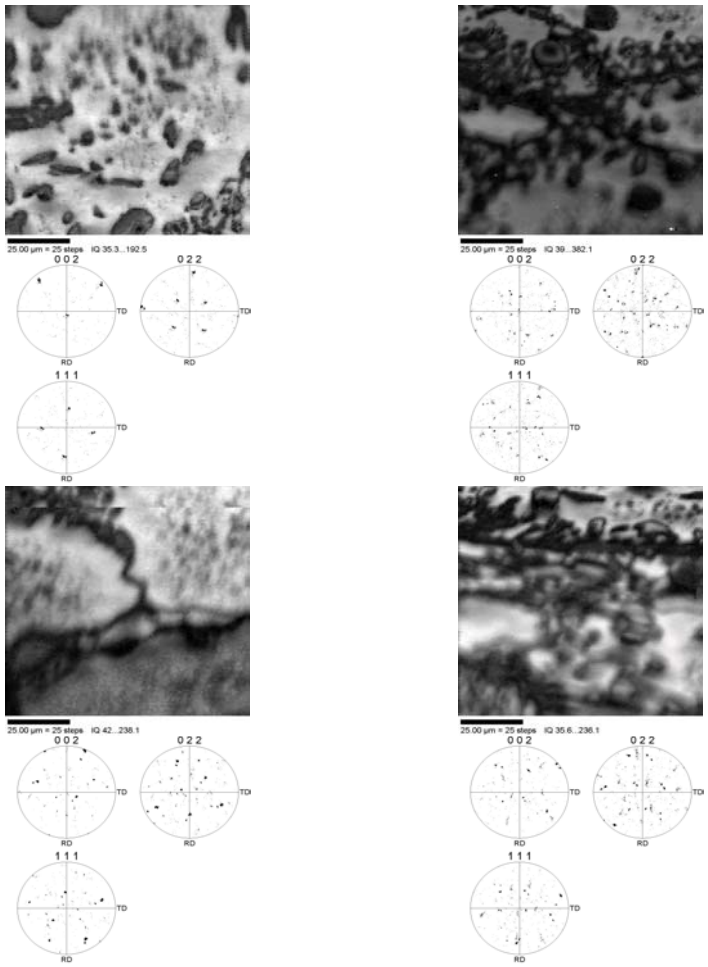

Figure 4.13 Sample 13 rows d and e

Sample 13 is base metal located on the advancing side of the tool; thus, it is of little import. The data was collected in order to ensure completeness. However, one should note that some variation is evident along both the TD and RD directions.

C. SECONDARY DATA

Upon completion the gathering of data on the aforementioned samples additional data were obtained for a series of scans traversing the TMAZ on sample 5.

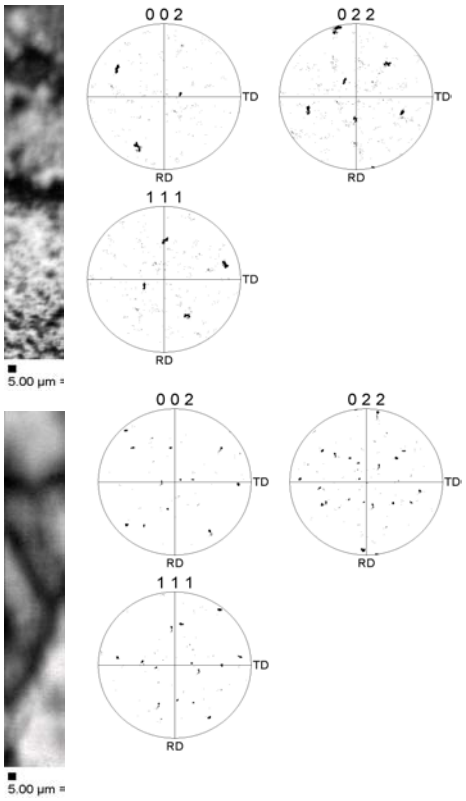

Figure 4.14 Top and Top/Middle of TMAZ (Sample 5)

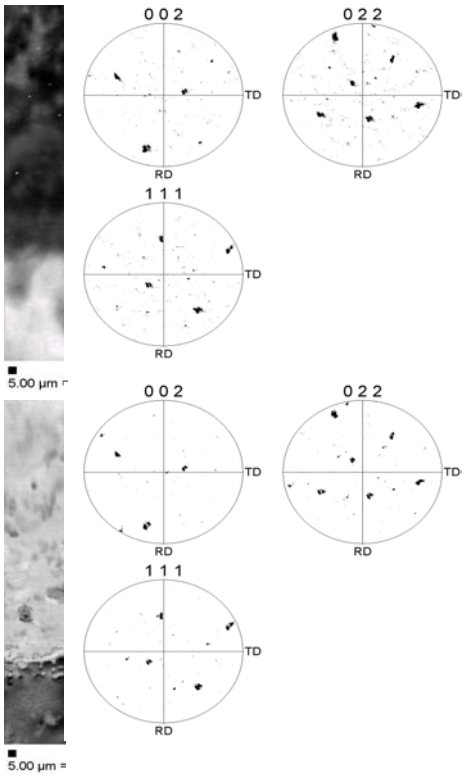

Figure 4.15 Bottom/Middle and Bottom of TMAZ (Sample 5)

Figures 4.14 and 4.15 show the data that was gathered from the top portion of sample 5. The scans were 200 micrometers in the RD direction by 50 micrometers along the TD direction. The data is intended to show the transition that NAB goes through when moving from TMAZ (top Figure 4.14) to base material (bottom Figure 4.15).

An additional sample was created that was identical to sample 7 with the exception that it included the void left in the material after the pin was withdrawn (see Figure 3.3). A series of 4 scans were performed on this sample starting from the void and moving in the TD/tool direction (see Figure 4.1). The scans, Figure 4.16, were 50 micrometers in the RD direction by 200 micrometers along the TD direction. This was done in an attempt to determine the pin's affect on the material before it. One can easily see a progression from the edge of the pin hole to the furthest scan (800 micrometers from the edge of the pin hole). This demonstrates that the pin causes disturbances in the material before actually traversing across it. This is most likely caused by the adiabatic heating and material displacement.

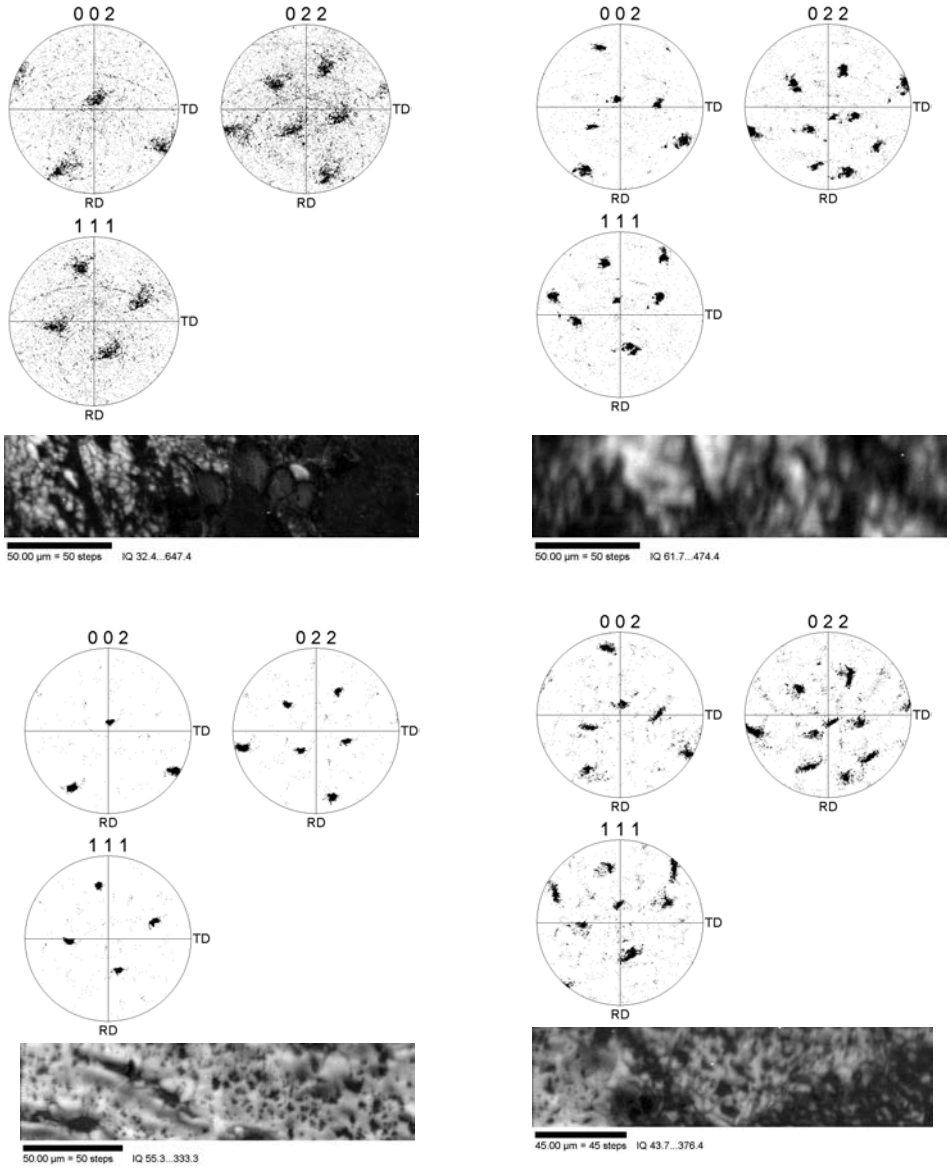

Figure 4.16 Tool Front Sample: The upper left image is the orientation data from 0-200 micrometers before the pin hole. The upper right image is 200-400 micrometers before the pin hole. The lower left image is 400-600 micrometers before the pin hole. The lower right image is 600-800 micrometers before the pin hole.

THIS PAGE INTENTIONALLY LEFT BLANK

V. SUMMARY AND CONCLUSIONS

A. SUMMARY AND CONCLUSIONS

The thermo-mechanically affected zone of friction stir processed NAB experiences severe plastic deformation coupled with affects due to the heat involved in the FSP process. The TMAZ is characterized by the presence of shear textures and moderately (10 micrometer) sized deformed grains. Grains located in the nugget are progressively smaller the closer they are to the center of the nugget. The following conclusions were drawn regarding shear textures in the TMAZ of friction stir processed NAB.

1. Primary Sample Data

(1) OIM is useful in determination and analysis of shear textures in highly deformed materials.

(2) C-type shear textures with {100} <110> slip systems were present in the lower region of the TMAZ from the lower retreating side corner to the lower advancing side corner. At these regions the shear or slip direction <110> was aligned in the direction of tool advance. Lattice orientations varied around this axis.

(3) Variation of grain orientation along the direction of tool travel was evident throughout the TMAZ and nugget.

(4) There are common orientations evident in transverse and longitudinal sections.

2. Extended Scans Sample 5

(1) Orientation data for a progression through the TMAZ into base metal on the retreating shoulder was gathered.

3. Tool Front Sample

(1) Orientation data for a progression through the TMAZ into base metal on the retreating shoulder was gathered and showed that the material was influenced by the pin’s travel out t a distance of 0.8mm.

B. RECOMMENDATIONS FOR FURTHER STUDY

Further investigation of the dynamics involved in the friction-stir process is needed. Ultimately this is necessary in order to properly understand the underlying physics involved in friction stir processing. Tensile test samples prepared from areas other than the center of the stir zone would be immensely useful. Conclusive corrosion tests on processed material could help prevent/understand possible material corrosion loss associated with the process. Additionally, sample conditions other than the 676 800/6 condition need to be explored.

LIST OF REFERENCES

1. Duma, J.A., “Heat Treatments For Optimizing Mechanical and Corrosion Resisting Properties of Nickel-Aluminum Bronzes,” *Naval Engineers Journal*, v. 87, p. 45-64, 1975.

2. Metals Handbook, 9th Ed., v. 2, Properties & Selections: Nonferrous Alloys and Pure Metals.

3. Military Specifications For Bronze, Nickel-Aluminum (UNS C95800), Castings For Seawater Service (MIL-B-24480A), 20 June 1985.

4. American Society for Testing and Materials (ASTM) B148 – 93a, Standard Specification for Aluminum-Bronze Sand Castings.

5. Sahoo, M., “Structure and Mechanical Properties of Slow-Cooled Nickel-Aluminum Bronze Alloy C95800,” *AFS Trans*, v. 90, p. 913-926, 1982.

6. Culpan, E.A. and Rose, G., “Corrosion Behavior of Cast Nickel Aluminum Bronze in Sea Water,” *British Corrosion Journal,* v. 14, p. 160-166, 1979.

7. A.M. Cuevas, Master’s Thesis, “Microstructure Characterization of Friction-Stir Processed Nickel-Aluminum Bronze through Orientation Imaging Microscopy,” Naval Postgraduate School, Monterey, CA, 2002.

8. W.M. Thomas, E.D. Nicholas, J.C. Needham, M.G. Murch, P. Templesmith and C.J. Dawes, “Friction Stir Butt Welding,” G.B. Patent Application No. 9125978.8, Dec. 1991; U.S. Patent No. 5460317, Oct. 1995.

9. Mishra, R.S. and Mahoney, M.W., “Friction Stir Processing: A New Grain Refinement Technique to Achieve High Strain Rate Superplasticity in Commercial Alloys,” *Materials Science Forum,* v. 357-359, p. 507-514, 2001.

10. P.B. Berbon, W.H. Bingel, R.S. Mishra, C.C. Bampton and M.W. Mahoney, “Friction Stir Processing: A Tool to Homogenize Nanocomposite Aluminum Alloys,” *Scripta Materialia*, v. 44, p. 61-66, 2001.

11. R.S. Mishra, M.W. Mahoney, S.X. McFadden, N.A. Mara and A.K. Mukherjee, “High Strain Rate Superplasticity In A Friction Stir Processed 7075 Al Alloy,” *Scripta Materialia*, v. 42, p. 163-168, 2000.

12. Weston, G.M., “Survey of Nickel-Aluminum-Bronze Casting Alloys on Marine Applications,” Australia Dept. of Defense Report, DSTO MRL, Melbourne, Victoria, MRL-R-807, 1981.

13. Weill-Couly, P. and Arnaud D., “Influence De La Composition Et De La Structure Des Cupro-Aluminiums Sur Leur Comportment En Service,” *Fonderie*, no. 322, p. 123-135, 1973.

14. Culpan, E.A. and Rose, G., “Microstructural Characterization Of Cast Nickel Aluminum Bronze,” *Journal of Materials Science*, v. 13, p. 1647-1657, 1978.

15. F. Hasan, A. Jahanafrooz, G.W. Lorimer and N. Ridley, “The Morphology, Crystallography, and Chemistry of Phases in As-Cast Nickel-Aluminum Bronze,” *Met. Trans A*, v. 13a, p.1337-1345, 1982.

16. A. Jahanafrooz, F. Hasan, G.W. Lorimer and N. Ridley, “Microstructural Development in Complex Nickel-Aluminum Bronze,” *Met. Trans A*, v. 14a, p. 1951-1956, 1983.

17. D.E. Bell, MS Thesis, “Microstructural Development and Corrosion Resistance of Laser-Welded Nickel-Aluminum Bronze,” Pennsylvania State University, PA, 1994.

18. Private communications, M.W. Mahoney, Rockwell Science Center, Thousand Oaks, CA, November 2002.

19. F. Hasan, A. Jahanafrooz, G.W. Lorimer and N. Ridley, “The Morphology, Crystallography, and Chemistry of Phases in As-Cast Nickel-Aluminum Bronze,” *Met. Trans A*, v. 13a, p.1337-1345, 1982.

20. G.R. Canova, U.F. Kocks and J.J. Jonas, “Theory of Torsion Texture Development,” *Acta Metall.*, v. 32, p. 211-226, 1984.

21. Brezina, P, “Heat Treatment of Complex Aluminum Bronzes,” *Int. Met. Rev.*, v. 27, n. 2, p. 77-120, 1982.

22. Orientation Imaging Microscopy (OIM) Data Collection User Manual, ver. 1.0, TexSEM Laboratories, Inc., 1998.

23. Orientation Imaging Microscopy (OIM) Analysis, ver. 3.0, TexSEM Laboratories, Inc., 2000.

24. D.P. Field, T.W. Nelson, Y. Hovanski and K.V. Jata, “Heterogeneity of Crystallographic Texture in Friction Stir Welds of Aluminum,” *Met. And Mat. Trans. A*, v. 32a, p. 2869-2877, 2001.

25. D.L. Swisher, MS Thesis, “Production of Ultra-Fine Grains and Evolution of Grain Boundaries During Severe Plastic Deformation of Aluminum and its Alloys,” Naval Postgraduate School, Monterey, CA, 2000.

26. S.D. Terhune, Z. Horita, M. Nemoto, Y. Li, T.G. Langdon and T.R. McNelley, ”The Evolution of Microtexture and Grain Boundary Character during ECA Pressing of Pure Aluminum,” *Intl. Conf. On Recrystallization and Related Phenomena*, p. 515-522, 1999.

27. A. Askari, Boeing INC., Private Communication June 2003

THIS PAGE INTENTIONALLY LEFT BLANK

INITIAL DISTRIBUTION LIST

1. Defense Technical Information Center
   Ft. Belvoir, Virginia

2. Dudley Knox Library
   Naval Postgraduate School
   Monterey, California

3. Engineering and Technology Curricular Office, Code 34
   Naval Postgraduate School
   Monterey, California

4. Department Chairman, Code ME/Kw
   Naval Postgraduate School
   Monterey, California

5. Professor Terry R. McNelley, Code ME/Mc
   Naval Postgraduate School
   Monterey, California

6. ENS Kenneth B Faires
   Hickory, North Carolina

7. Dr. Leo Christodoulou
   DARPA/DSO
   Arlington, Virginia

8. Murray W. Mahoney
   Rockwell Science Center
   Thousand Oaks, California

9. William Palko
   Naval Surface Warfare Center
   Carderock Division
   West Bethesda, Maryland